Dependence Between Parameter Estimation and Statistical Hypothesis Testing Positioning Safety Analysis for Automated/Autonomous Vehicles

Ciuban, Sebastian; Teunissen, Peter J.G.; Tiberius, Christian C.J.M.

DOI
10.1109/TITS.2025.3528995

Publication date
2025

Document Version
Final published version

Published in
IEEE Transactions on Intelligent Transportation Systems

Dependence Between Parameter Estimation and Statistical Hypothesis Testing: Positioning Safety Analysis for Automated/Autonomous Vehicles

Sebastian Ciuban, Peter J. G. Teunissen, *Senior Member, IEEE*, and Christian C. J. M. Tiberius

***Abstract*— The analysis of positioning safety often employs a probability-based formulation. This approach quantifies the probability of positioning failure, which is the probability of the position estimator being outside a safety-region, and compares it against an application specific requirement. The design of positioning algorithms for safety-critical applications, such as automated/autonomous vehicles, should consider the dependence between parameter or state estimation and statistical hypothesis testing for model misspecifications in the evaluation of positioning safety. If this dependence is not considered, as this article shows, the conclusions drawn from the positioning safety analysis might be overly-optimistic. Therefore, this article focuses on the aforementioned dependence through a vehicle positioning scenario based on an Extended Kalman Filter (EKF) and the Detection, Identification, and Adaptation (DIA) method for misspecifications in the motion and measurement models. Grounded in the distributional theory for the DIA method, our positioning safety analysis utilizes the conditional probability density functions (PDFs) of the combined EKF and DIA position error, which are generally nonnormal. We compute the probability of vehicle positioning failure in two cases 1) when the dependence is considered and 2) when it is not, to quantify the over-optimism introduced by ignoring this dependence. Finally, we present our conclusions and recommendations.**

***Index Terms*— Positioning safety, probability of positioning failure, DIA method, conditional PDFs, automated driving.**

I. Introduction

PARAMETER or state estimation and statistical hypothesis testing for model misspecifications are two central statistical inference tools in the design of positioning systems for safety-critical applications, such as automated/autonomous vehicles [1], [2], [3]. Given a chosen parameter estimation and statistical hypothesis testing procedure, along with the obtained n-dimensional position estimation error $\underline{\overline{\epsilon}} \in \mathbb{R}^n$ of a vehicle and an application-specific safety region $\mathcal{B} \subset \mathbb{R}^n$, the event of positioning failure can be formulated as $\mathcal{F} = \{\underline{\overline{\epsilon}} \notin \mathcal{B}\}$ [4]. For positioning safety analyses the *probability of positioning failure* (denoted as $\mathbb{P}_{\mathcal{F}}$) can be used to verify whether requirements or guidelines are being met (e.g., the ones in [5]). The probability of positioning failure can be expressed as,

$$\mathbb{P}_{\mathcal{F}} = \int_{\mathcal{B}^c} f_{\underline{\overline{\epsilon}}}(e)\, de, \tag{1}$$

where $f_{\underline{\overline{\epsilon}}}(\epsilon)$ is the probability density function (PDF) of $\underline{\overline{\epsilon}} \in \mathbb{R}^n$ and $\mathcal{B}^c \subset \mathbb{R}^n$ is the complement of the safety-region $\mathcal{B} \subset \mathbb{R}^n$. Such probability-based formulations, along with the computation or upperbounding of these probabilities, are widely used for safety analyses of failure events in nuclear power plants, aerospace systems, structural engineering, and Global Navigation Satellite System (GNSS) based positioning for civil aviation applications [6], [7], [8], [9], [10], [11]. The application of similar principles from GNSS-based positioning in civil aviation has also been discussed for automated/autonomous vehicles in [3], [12], and [13].

Since both parameter estimation and statistical hypothesis testing are used in the algorithms of positioning systems, the dependence between them should be reflected in the PDF $f_{\underline{\overline{\epsilon}}}(\epsilon)$ [14], [15], [16], [17], [18], [19], [20], [21], [22], [23], [24]. To the best of the authors' knowledge, there is a lack of positioning safety analyses for automated/autonomous vehicles that specifically address the dependence between parameter estimation and statistical hypothesis testing when quantifying $\mathbb{P}_{\mathcal{F}}$. Therefore, we put forward the following question in the context of positioning safety analyses for automated/autonomous vehicles:

How do the results for $\mathbb{P}_{\mathcal{F}}$ differ when the dependence between parameter estimation and statistical hypothesis testing is accounted for, compared to when it is ignored?

In this article, we show through a positioning scenario of an automated vehicle, driving cooperatively with an adjacent vehicle, that ignoring the aforementioned dependence can result in its $\mathbb{P}_{\mathcal{F}}$ being one order of magnitude too optimistic. The consequence of this over-optimism is that it may lead to safety requirements or guidelines being declared satisfied when they are not.

For vehicle positioning, we use an Extended Kalman Filter (EKF) for parameter (or state) estimation [25], [26], along with the Detection, Identification, and Adaptation (DIA) procedure to perform statistical hypothesis testing to accommodate for multiple model misspecifications [14], [27]. Examples of model misspecifications are unmodelled accelerations in

Received 15 April 2024; revised 30 October 2024; accepted 31 December 2024. This work was supported by the Dutch Research Council (NWO) under Grant 18305 through I-GNSS Positioning for Assisted and Automated Driving. The Associate Editor for this article was L. Li. *(Corresponding author: Sebastian Ciuban.)*

The authors are with the Department of Geoscience and Remote Sensing, Delft University of Technology, 2628 CN Delft, The Netherlands (e-mail: ciuban.sebastian@gmail.com; p.j.g.teunissen@tudelft.nl; c.c.j.m.tiberius@tudelft.nl).

Digital Object Identifier 10.1109/TITS.2025.3528995

the vehicle's motion model, outliers and anomalies which may incidentally corrupt sensor measurements (e.g., from a GNSS receiver), etc. To account for the dependence between parameter estimation and statistical hypothesis testing in the PDF $f_{\bar{\underline{\epsilon}}}(\epsilon)$ of the estimation error $\bar{\underline{\epsilon}} \in \mathbb{R}^n$ we apply the principles of the theoretical framework introduced recently in [14]. Building on this setup, we proceed with the positioning safety analysis based on $\mathbb{P}_{\mathcal{F}}$ during design stage of the positioning systems (i.e., offline). At the design stage, decisions are made regarding (i) measurement models, (ii) parameter estimation methods, (iii) statistical hypothesis testing procedures to accommodate for model misspecifications (e.g., missmodeling of the vehicles' motion, outliers or faults in sensor measurements), and (iv) positioning scenarios for vehicles, among other factors. This approach aligns with the scenario-based safety assessment framework used for automated and autonomous vehicles [28], [29], [30].

This article is organized as follows: In Section II we present the combined Kalman Filter (KF) and DIA method, while discussing the principles of approaching statistical hypothesis testing through the partitioning of the vector space of KF-predicted residuals. These principles, though illustrated with the KF and DIA method, are equally applicable to the EKF and DIA method. In Section III we show the expression of the PDF $f_{\bar{\underline{\epsilon}}}(\epsilon)$ which accounts for the dependence between the (E)KF and the DIA method. Section III further shows: (i) the formulation of the probability of positioning failure based on $f_{\bar{\underline{\epsilon}}}(\epsilon)$ and its conditional components resulted from the application of the rule of total probability; (ii) the formulation of the probability of positioning failure when the aforementioned dependence is *ignored*. Section IV presents, by means of an example, a quantitative positioning safety analysis for an automated vehicle driving cooperatively with an adjacent vehicle. First, we carry out an analysis based on the components of the PDF $f_{\bar{\underline{\epsilon}}}(\epsilon)$ which is used to determine which of these components have the largest (or smallest) impact on the probability of positioning failure. Secondly, we compare the obtained results with the case when the aforementioned dependence is ignored and quantify the difference. Finally, we present our conclusions and recommendations in Section V.

Throughout the paper we make use of the following notation: an underscore denotes a random quantity (e.g., the random vector $\underline{\mathrm{x}} \in \mathbb{R}^n$), $f_{\underline{\mathrm{x}}}(x)$ is the PDF of $\underline{\mathrm{x}}$, $\mathsf{E}(\underline{\mathrm{x}})$ is the expectation, $\mathsf{D}(\underline{\mathrm{x}})$ is the dispersion or variance operator, and $\mathsf{C}(\underline{\mathrm{x}}, \underline{\mathrm{y}})$ is the covariance operator. The error-variance matrices are denoted with a capital italic P while the probability of an event $\mathcal{E}$ is denoted $\mathsf{P}_{\mathcal{E}} = \mathsf{P}(\mathcal{E})$. For the weighted squared norm of a vector we use the notation $||.||^2_Q = (.)^T Q^{-1}(.)$. We also provide Table I with the notation for key symbols.

TABLE I
KEY SYMBOLS AND THEIR DESCRIPTION

Symbol	Description
$\underline{\nu}$	Vector of predicted residuals
$Q_{\nu\nu}$	Variance-covariance matrix of $\underline{\nu}$
$f_{\underline{\nu}}(\nu)$	PDF of $\underline{\nu}$
$\mathcal{H}_i$	Hypothesis i
$f_{\underline{\nu}}(\nu\|\mathcal{H}_i)$	PDF of $\underline{\nu}$ under $\mathcal{H}_i$
C_i	Vector/matrix of model misspecification under a $\mathcal{H}_i$
$\mathcal{R}(C_i)$	Range space of C_i
$\mathbf{Q}_{C_i}$	Projection matrix onto the range space of C_i
$\mathcal{P}_i$	Partition i of the predicted residuals vector space
L_i	Term adapting the model under $\mathcal{H}_0$ to $\mathcal{H}_{i\neq 0}$
b_i	Size of the model misspecification
q_i	Dimension of $b_i \in \mathbb{R}^{q_i}$
$\hat{\underline{\epsilon}}_i$	Filter error of the (E)KF using the models under $\mathcal{H}_i$
$\bar{\underline{\epsilon}}$	Filter error of the combined (E)KF and DIA method
$f_{\bar{\underline{\epsilon}}}(\epsilon\|\mathcal{H}_i)$	PDF of $\bar{\underline{\epsilon}}$ under $\mathcal{H}_i$
$f_{\bar{\underline{\epsilon}}\|\mathcal{E}}(\epsilon\|\mathcal{E})$	PDF of $\bar{\underline{\epsilon}}$ conditioned on the event $\mathcal{E}$
$\mathcal{B}$	Safety-region of the vehicle
$\mathbb{P}_{\mathcal{F}}$	Probability of positioning failure
$\mathbb{P}_{\mathcal{F}}\|\mathcal{H}_i$	$\mathbb{P}_{\mathcal{F}}$ under $\mathcal{H}_i$
$\mathbb{P}_{\mathcal{F}}\|\mathcal{E}$	$\mathbb{P}_{\mathcal{F}}$ conditioned on the event $\mathcal{E}$

II. Combined Kalman Filter and DIA Method

The discrete-time evolution of the state vector $\underline{\mathrm{x}}_k \in \mathbb{R}^n$ (at epoch k) can be captured by the linear(ized) motion model

$$\underline{\mathrm{x}}_k = \Phi_{k,k-1}\underline{\mathrm{x}}_{k-1} + \underline{\mathrm{d}}_k, \tag{2}$$

where $\Phi_{k,k-1} \in \mathbb{R}^{n\times n}$ denotes the transition matrix, $\underline{\mathrm{d}}_k \in \mathbb{R}^n$ is the process noise which is assumed to have a normal distribution with $\mathsf{E}(\underline{\mathrm{d}}_k) = 0_{n\times 1}$, $\mathsf{C}(\underline{\mathrm{d}}_k, \underline{\mathrm{d}}_l) = Q_{\mathrm{d}_k\mathrm{d}_k}\delta_{kl}$, and $\mathsf{C}(\underline{\mathrm{d}}_k, \underline{\mathrm{x}}_{\mathrm{init}}) = 0_{n\times n}$ with δ_{kl} being the Kronecker delta and $\underline{\mathrm{x}}_{\mathrm{init}}$ is the normally distributed initial state vector.

The following linear(ized) measurement model describes the relation between the random vector of observables $\underline{\mathrm{y}}_k \in \mathbb{R}^{m_k}$ and $\underline{\mathrm{x}}_k$,

$$\underline{\mathrm{y}}_k = A_k\,\underline{\mathrm{x}}_k + \underline{\mathrm{e}}_k, \tag{3}$$

where $A_k \in \mathbb{R}^{m_k\times n}$ is the design matrix and $\underline{\mathrm{e}}_k \in \mathbb{R}^{m_k}$ is the measurement noise which is assumed to have a normal distribution with $\mathsf{E}(\underline{\mathrm{e}}_k) = 0_{m_k\times 1}$, $\mathsf{C}(\underline{\mathrm{e}}_k, \underline{\mathrm{e}}_l) = R_k\delta_{kl}$, $\mathsf{C}(\underline{\mathrm{e}}_k, \underline{\mathrm{x}}_{\mathrm{init}}) = 0_{m_k\times n}$, and $\mathsf{C}(\underline{\mathrm{e}}_k, \underline{\mathrm{d}}_k) = 0_{m_k\times n}$.

Misspecifications could occur in the functional and stochastic models from (2) and (3). We consider the case of misspecifications only in the functional models as these are the most common occurring in practice [31]. In subsequent developments, we omit the k index for simplicity. Based on the vector of predicted residuals $\underline{\nu} \in \mathbb{R}^m$ (Figure 1), a DIA procedure can be designed [27], [31], [32], [33]. The multiple statistical hypothesis testing problem is

$$\mathcal{H}_0 : \mathsf{E}(\underline{\nu}) = 0_{m\times 1} \quad \text{vs.} \quad \mathcal{H}_{i\neq 0} : \mathsf{E}(\underline{\nu}) = C_i b_i, \tag{4}$$

for $i \in \{1, \ldots, n_{\mathcal{H}}\}$, where $C_i \in \mathbb{R}^{m\times q_i}$ has $\mathrm{rank}(C_i) = q_i$ for $i \neq 0$. The matrix C_i specifies the type of model misspecification (e.g., unmodelled accelerations, outliers in sensor measurements), $b_i \in \mathbb{R}^{q_i}$ is the size of the model misspecification and $q_i \in \{1, \ldots, m\}$ is its dimension for $i \neq 0$. It is possible to unambiguously link the testing decisions for the $\mathcal{H}_i$'s to partitions $\mathcal{P}_i$ of vector space $\mathbb{R}^m$ such that $\cup_{i=0}^{n_{\mathcal{H}}} \mathcal{P}_i = \mathbb{R}^m$ and $\mathcal{P}_i \cap \mathcal{P}_j = \emptyset$ for $i \neq j$. Therefore, if the predicted residual $\underline{\nu}$ lands in a $\mathcal{P}_i \subset \mathbb{R}^m$ (i.e., $\underline{\nu} \in \mathcal{P}_i$) then hypothesis $\mathcal{H}_i$ is selected as most likely. The equations of the KF together with the local Detection ($\mathcal{D}$) Identification ($\mathcal{I}$) and Adaptation ($\mathcal{A}$) procedure are shown in Figure 1. The initialization of the KF is done according to Lemma 7 in [34] yielding $\hat{\underline{\mathrm{x}}}_{\mathrm{init}}$ and its error-variance matrix P_{init}.

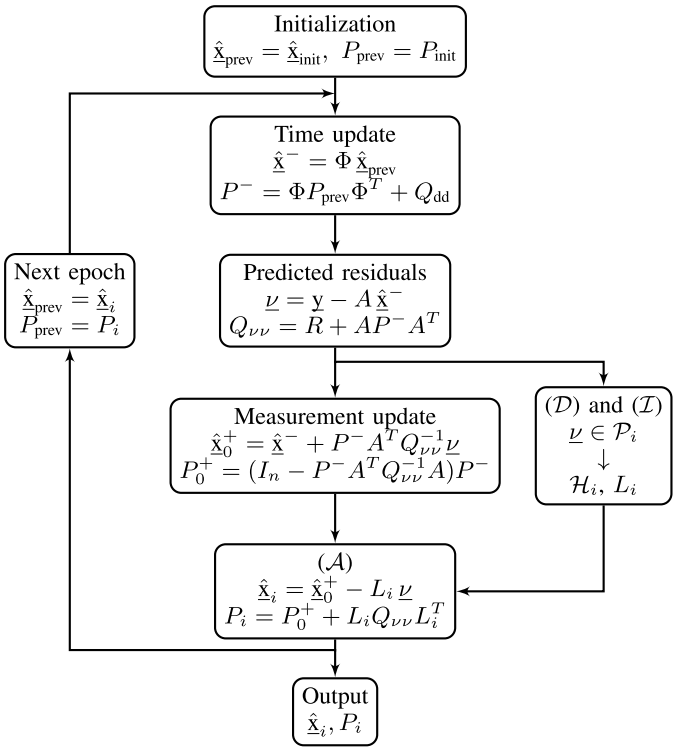

Fig. 1. KF equations and DIA procedure. Time updated variables have the $[.]^-$ superscript and the measurement updated ones have $[.]^+$. The subscript $[.]_0$ indicates the vector or matrix using the models of $\mathcal{H}_0$. The $L_i \in \mathbb{R}^{n\times m}$ (given in the Appendix) drives the adaptation step under a $\mathcal{H}_{i\neq 0}$ and $L_i = 0$ for $i = 0$.

The *combined* outcome of the KF and of the DIA procedure is expressed as

$$\underline{\bar{x}} = \sum_{i=0}^{n_{\mathcal{H}}} \underline{\hat{x}}_i\, p_i(\underline{\nu}), \tag{5}$$

where $p_i(\underline{\nu})$ is an indicator function which takes the value 1 if $\underline{\nu} \in \mathcal{P}_i$, and 0 otherwise. Note that the uncertainty of (5) is driven by $\underline{\hat{x}}_i$ and by $p_i(\underline{\nu})$. The definitions of the partitions are (an example is shown in Figure 2)

$$\begin{aligned}\mathcal{P}_0 &= \left\{\nu \in \mathbb{R}^m \mid ||\nu||^2_{Q_{\nu\nu}} \leq \chi^2_\alpha(m,0)\right\},\\ \mathcal{P}_{i\neq 0} &= \left\{\nu \in \mathbb{R}^m \mid \nu \notin \mathcal{P}_0,\ \breve{\mathsf{T}}_i = \max_{j\in\{1,\ldots,n_{\mathcal{H}}\}} \mathsf{T}_j\right\},\end{aligned} \tag{6}$$

where $||\underline{\nu}||^2_{Q_{\nu\nu}}$ is the overall model test statistic, $\chi^2_\alpha(m,0)$ is the Chi-squared critical value for a level of significance α, and $\underline{\mathsf{T}}_j$ is the result of the following transformation [31], [35]

$$\underline{\mathsf{T}}_j = \text{CDF}_{\chi^2(q_j,0)}\left(||\mathbf{Q}_{C_j}\underline{\nu}||^2_{Q_{\nu\nu}}\right), \tag{7}$$

where $\text{CDF}_{\chi^2(q_j,0)}(.)$ is the cumulative distribution function (CDF) of $\chi^2(q_j,0)$, $||\mathbf{Q}_{C_j}\underline{\nu}||^2_{Q_{\nu\nu}} \overset{\mathcal{H}_0}{\sim} \chi^2(q_j,0)$, $\mathbf{Q}_{C_j} = C_j\left(C_j^TQ_{\nu\nu}^{-1}C_j\right)^{-1}C_j^TQ_{\nu\nu}^{-1}$ is a projection matrix onto $\mathcal{R}(C_j)$, and $\underline{\mathsf{T}}_l$ has a uniform distribution on the interval $[0,1]$ under $\mathcal{H}_0$. This transformation is applied such that all $\underline{\mathsf{T}}_j$ have the same PDF under $\mathcal{H}_0$ as the dimension of the model misspecification $b_i \in \mathbb{R}^{q_i}$ would generally differ

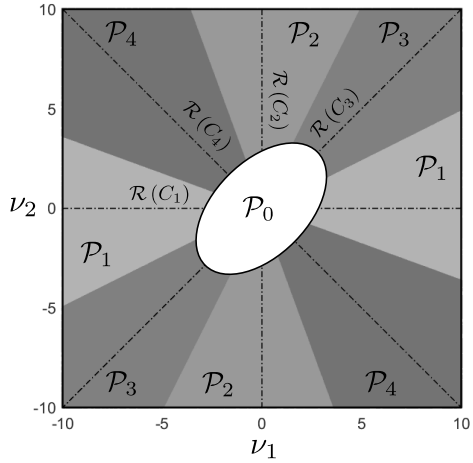

Fig. 2. Example of partitioning predicted residual vector space $\mathbb{R}^{m=2}$ when $\underline{\nu} \sim \mathcal{N}(\mathsf{E}(\underline{\nu}), Q_{\nu\nu})$, $Q_{\nu\nu} = \begin{bmatrix}2 & 1\\ 1 & 2\end{bmatrix}$, $\mathcal{H}_0 : \mathsf{E}(\underline{\nu}) = 0_{m\times 1}$, $\mathcal{H}_{i\neq 0} : \mathsf{E}(\underline{\nu}) = C_ib_i$, $i \in [1,4]$, and $\alpha = 10^{-1}$. The following types of 1D model misspecifications are considered: $C_1 = [1\ 0]^T$, $C_2 = [0\ 1]^T$, $C_3 = [1\ 1]^T$, and $C_4 = [1\ -1]^T$. The dotted lines are the vector spaces spanned by $\mathcal{R}(C_i) \subset \mathbb{R}^{m=2}$.

across $\mathcal{H}_{i\neq 0}$. Therefore, $\breve{\underline{\mathsf{T}}}_i$ corresponds to the most likely $\mathcal{H}_{i\neq 0}$. Equation (5) together with (6) describe the following procedure

$$\begin{cases}\text{if } \underline{\nu} \in \mathcal{P}_0 \text{ (no } \mathcal{D}) \rightarrow \text{output } \underline{\hat{x}}_0,\\ \text{if } \underline{\nu} \notin \mathcal{P}_0\ (\mathcal{D}) \rightarrow \underline{\nu} \in \mathcal{P}_{i\neq 0}\ (\mathcal{I}) \rightarrow \text{output } \underline{\hat{x}}_i\ (\mathcal{A}).\end{cases} \tag{8}$$

III. Conditional PDFs and Total Probability of Positioning Failure

From (5) is clear that $p_i(\underline{\nu})$ defines a nonlinear mapping of $\underline{\nu}$ which causes the PDF of the filter error $\underline{\bar{\epsilon}} = \underline{x} - \underline{\bar{x}}$ *to not be normally distributed* despite that $\underline{\hat{\epsilon}}_i \sim \mathcal{N}(0_{n\times 1},\ P_i)$. The PDF of $\underline{\bar{\epsilon}}$ follows from Theorem 1 in [14]

$$\begin{aligned}f_{\underline{\bar{\epsilon}}}(\epsilon) &= \sum_{i=0}^{n_{\mathcal{H}}}\int_{\mathcal{P}_i} f_{\underline{\hat{\epsilon}}_i,\underline{\nu}}(\epsilon,\upsilon)d\upsilon\\ &= \sum_{i=0}^{n_{\mathcal{H}}}\int_{\mathcal{P}_i} f_{\underline{\hat{\epsilon}}_0}(\epsilon + L_i\upsilon)\, f_{\underline{\nu}}(\upsilon)d\upsilon,\end{aligned} \tag{9}$$

where use has been made of the independence between the normally distributed $\underline{\hat{\epsilon}}_0$ and $\underline{\nu}$ [34]. However, $\underline{\hat{\epsilon}}_i$ and $\underline{\nu}$ are *dependent* since the joint PDF $f_{\underline{\hat{\epsilon}}_i,\underline{\nu}}(\epsilon,\nu) \neq f_{\underline{\hat{\epsilon}}_i}(\epsilon)f_{\underline{\nu}}(\nu)$ for $i > 0$ [14]. One can decompose (9) via the rule of total probability to obtain the conditional PDFs which account for the testing decisions under $\mathcal{H}_0$, such as Correct Acceptance (CA) when $\mathcal{H}_0$ is accepted and False Alarm (FA_i) when $\mathcal{H}_0$ is rejected and $\mathcal{H}_i$ is accepted,

$$f_{\underline{\bar{\epsilon}}}(\epsilon|\mathcal{H}_0) = f_{\underline{\bar{\epsilon}}|\text{CA}}(\epsilon|\text{CA})\mathsf{P}_{\text{CA}} + \sum_{i=1}^{n_{\mathcal{H}}} f_{\underline{\bar{\epsilon}}|\text{FA}_i}(\epsilon|\text{FA}_i)\,\mathsf{P}_{\text{FA}_i}, \tag{10}$$

where $f_{\underline{\bar{\epsilon}}|\text{CA}}(\epsilon|\text{CA}) = f_{\underline{\hat{\epsilon}}_0}(\epsilon|\mathcal{H}_0) = \mathcal{N}(0_{n\times 1},\ P_0)$ and

$$f_{\underline{\bar{\epsilon}}|\text{FA}_i}(\epsilon|\text{FA}_i) = \frac{\int_{\mathcal{P}_i} f_{\underline{\hat{\epsilon}}_0}(\epsilon + L_i\upsilon|\mathcal{H}_0)\, f_{\underline{\nu}}(\upsilon|\mathcal{H}_0)d\upsilon}{\mathsf{P}_{\text{FA}_i}} \tag{11}$$

for $i > 0$, $\mathsf{P}_{\mathrm{CA}} = \mathsf{P}\left(\underline{\nu} \in \mathcal{P}_0 | \mathcal{H}_0\right)$, $\mathsf{P}_{\mathrm{FA}_i} = \mathsf{P}\left(\underline{\nu} \in \mathcal{P}_i | \mathcal{H}_0\right)$ are the probabilities of the events of CA and FA_i such that $\mathsf{P}_{\mathrm{FA}} = \sum_{i=1}^{n_{\mathcal{H}}} \mathsf{P}_{\mathrm{FA}_i}$ and $1 = \mathsf{P}_{\mathrm{CA}} + \mathsf{P}_{\mathrm{FA}}$. The summation term in (10) causes $f_{\underline{\epsilon}}(\epsilon|\mathcal{H}_0)$ to be a nonnormal PDF. Similarly, under an alternative hypothesis $\mathcal{H}_a$ the decomposition of (9) gives the following result based on the testing decisions: Missed Detection (MD_a) when $\mathcal{H}_0$ is accepted, Correct Identification (CI_a) when $\mathcal{H}_0$ is rejected and $\mathcal{H}_a$ is accepted, and Wrong Identification (WI) when $\mathcal{H}_0$ is rejected and $\mathcal{H}_j$ is accepted for $j \notin \{0, a\}$,

$$f_{\underline{\epsilon}}(\epsilon|\mathcal{H}_a) = f_{\underline{\epsilon}|\mathrm{MD}_a}(\epsilon|\mathrm{MD}_a)\mathsf{P}_{\mathrm{MD}_a} + f_{\underline{\epsilon}|\mathrm{CI}_a}(\epsilon|\mathrm{CI}_a)\,\mathsf{P}_{\mathrm{CI}_a} + \sum_{i\neq 0,a}^{n_{\mathcal{H}}} f_{\underline{\epsilon}|\mathrm{WI}_i}(\epsilon|\mathrm{WI}_i)\,\mathsf{P}_{\mathrm{WI}_i}, \quad (12)$$

where $f_{\underline{\epsilon}|\mathrm{MD}_a}(\epsilon|\mathrm{MD}_a) = f_{\underline{\hat{\epsilon}}_0}(\epsilon|\mathcal{H}_a) = \mathcal{N}(L_a C_a b_a, P_0)$,

$$f_{\underline{\epsilon}|\mathrm{CI}_a}(\epsilon|\mathrm{CI}_a) = \frac{\int_{\mathcal{P}_a} f_{\underline{\hat{\epsilon}}_0}(\epsilon + L_a\upsilon|\mathcal{H}_a)\, f_{\underline{\nu}}(\upsilon|\mathcal{H}_a)d\upsilon}{\mathsf{P}_{\mathrm{CI}_a}},$$
$$f_{\underline{\epsilon}|\mathrm{WI}_i}(\epsilon|\mathrm{WI}_i) = \frac{\int_{\mathcal{P}_i} f_{\underline{\hat{\epsilon}}_0}(\epsilon + L_i\upsilon|\mathcal{H}_a)\, f_{\underline{\nu}}(\upsilon|\mathcal{H}_a)d\upsilon}{\mathsf{P}_{\mathrm{WI}_i}}, \quad (13)$$

with $\mathsf{P}_{\mathrm{MD}_a} = \mathsf{P}\left(\underline{\nu} \in \mathcal{P}_0|\mathcal{H}_a\right)$, $\mathsf{P}_{\mathrm{CI}_a} = \mathsf{P}\left(\underline{\nu} \in \mathcal{P}_a|\mathcal{H}_a\right)$, and $\mathsf{P}_{\mathrm{WI}_i} = \mathsf{P}\left(\underline{\nu} \in \mathcal{P}_i|\mathcal{H}_a\right)$ for $i \notin \{0, a\}$ being the probabilities of the events of MD_a, CI_a, and WI_j such that $1 = \mathsf{P}_{\mathrm{MD}_a} + \mathsf{P}_{\mathrm{CI}_a} + \sum_{i\neq 0,a}^{n_{\mathcal{H}}} \mathsf{P}_{\mathrm{WI}_i}$. The second and third terms in (12) cause $f_{\underline{\epsilon}}(\epsilon|\mathcal{H}_a)$ to be a nonnormal PDF.

Next, we formulate the total probability of positioning failure based on (10), (12), a given safety-region $\mathcal{B} \subset \mathbb{R}^n$, and its complement $\mathcal{B}^c = \mathbb{R}^n / \mathcal{B}$

$$\begin{aligned}\mathbb{P}_{\mathcal{F}}(\mathsf{b}) &= \int_{\mathcal{B}^c} f_{\underline{\epsilon}}(e)\, de \\ &= \omega_0 \int_{\mathcal{B}^c} f_{\underline{\epsilon}}(e|\mathcal{H}_0)\, de + \sum_{i=1}^{n_{\mathcal{H}}} \omega_i \left(\int_{\mathcal{B}^c} f_{\underline{\epsilon}}(e|\mathcal{H}_i)\, de\right) \\ &= \omega_0\, \mathbb{P}_{\mathcal{F}}|\mathcal{H}_0 + \sum_{i=1}^{n_{\mathcal{H}}} \omega_i\, (\mathbb{P}_{\mathcal{F}}|\mathcal{H}_i(b_i)), \end{aligned} \quad (14)$$

where the dependence on the size of the model misspecifications $\mathsf{b} = \{b_1,\ b_2\ , \ldots\ , b_{n_{\mathcal{H}}}\}$ has been accounted for in the notation, and $\omega_i = \mathsf{P}(\mathcal{H}_i)$ are the a-priori probabilities of occurrence of the hypotheses $\mathcal{H}_i$ for $i \in \{0, \ldots, n_{\mathcal{H}}\}$. A further decomposition of (14) via the rule of total probability gives

$$\begin{aligned}\mathbb{P}_{\mathcal{F}}(\mathsf{b}) = \omega_0(&\mathsf{P}_{\mathrm{CA}}\mathbb{P}_{\mathcal{F}}|\mathrm{CA} + \sum_{i=1}^{n_{\mathcal{H}}} \mathsf{P}_{\mathrm{FA}_i}\mathbb{P}_{\mathcal{F}}|\mathrm{FA}_i) \\ &+ \sum_{a=1}^{n_{\mathcal{H}}} \omega_a(\mathsf{P}_{\mathrm{MD}_a}\mathbb{P}_{\mathcal{F}}|\mathrm{MD}_a(b_a) + \mathsf{P}_{\mathrm{CI}_a}\mathbb{P}_{\mathcal{F}}|\mathrm{CI}_a(b_a) \\ &+ \sum_{i\neq 0,a}^{n_{\mathcal{H}}} \mathsf{P}_{\mathrm{WI}_i}\mathbb{P}_{\mathcal{F}}|\mathrm{WI}_i(b_a)), \end{aligned} \quad (15)$$

The decomposition(s) of $\mathbb{P}_{\mathcal{F}}(\mathsf{b})$ is useful in the design stage of the positioning system. It helps identify which hypotheses, along with the associated testing decision outcomes, have the largest impact or are most influential to $\mathbb{P}_{\mathcal{F}}(\mathsf{b})$. The evaluation of (15) is mainly driven by three factors: (i) the structure of the nonnormal conditional PDFs, (ii) the range of the model misspecifications inside the set b to find the worst-case $\mathbb{P}_{\mathcal{F}}(\mathsf{b})$, and (iii) the shape and size of the safety-region $\mathcal{B}$.

If, in the safety-analysis, one would *ignore* the dependence between parameter estimation and statistical hypothesis testing and assume $\underline{\hat{\epsilon}}_i$ and $\underline{\nu}$ to be *independent* for all $i \in \{0, \ldots, n_{\mathcal{H}}\}$ then (9) would become

$$f_{\underline{\epsilon}^o}(\epsilon) = \sum_{i=0}^{n_{\mathcal{H}}} f_{\underline{\hat{\epsilon}}_i}(\epsilon) \int_{\mathcal{P}_i} f_{\underline{\nu}}(\upsilon) d\upsilon, \quad (16)$$

where $f_{\underline{\hat{\epsilon}}_i,\underline{\nu}}(\epsilon, \nu) = f_{\underline{\hat{\epsilon}}_i}(\epsilon)\, f_{\underline{\nu}}(\nu)$ is expressed as a product of the marginal PDFs. Then the formulation of the probability of the positioning failure, when the aforementioned dependence is ignored, is based on

$$\mathbb{P}^o_{\mathcal{F}}(\mathsf{b}) = \int_{\mathcal{B}^c} f^o_{\underline{\epsilon}}(e)\, de, \quad (17)$$

and decompositions via the rule of total probability can similarly be done as in (14) and (15).

IV. Quantitative Safety Analysis for Cooperative Vehicle Positioning

To illustrate the principles from the previous sections we consider, as an example, the case of two connected vehicles driving on a highway in a cooperative positioning setting. The two-vehicles are capable of exchanging positional coordinates as provided by their positioning systems (e.g., via Cooperative Awareness Messages) and conduct inter-vehicle distance measurements (e.g., via LiDAR, Radar) [36], [37], [38]. Each vehicle runs an EKF which makes use of the cooperative positioning information to improve its positioning performance. In the following sub-sections we present the chosen motion and measurement models, the simulation scenario, and the results of the positioning safety-analysis for single and multiple configurations of the vehicles.

A. Motion and Measurement Models

Curvilinear motion models are commonly used for vehicle tracking [39], [40], [41]. Among them we choose the Constant Turn Rate and Velocity (CTRV) model given its suitability for highway driving conditions. The perturbed nonlinear equations of motion are

$$\underbrace{\begin{bmatrix}\dot{\underline{\mathsf{u}}}\\ \dot{\underline{\mathsf{v}}}\\ \dot{\underline{\mathsf{s}}}\\ \dot{\underline{\psi}}\\ \dot{\underline{\theta}}\end{bmatrix}}_{\dot{\underline{\mathrm{x}}}} = \underbrace{\begin{bmatrix}\mathsf{s}\cos(\psi)\\ \mathsf{s}\sin(\psi)\\ 0\\ \theta\\ 0\end{bmatrix}}_{\Phi(\mathrm{x})} + \underbrace{\begin{bmatrix}0 & 0\\ 0 & 0\\ 1 & 0\\ 0 & 0\\ 0 & 1\end{bmatrix}}_{G} \underbrace{\begin{bmatrix}\underline{z}_{\dot{\mathsf{s}}}\\ \underline{z}_{\dot{\theta}}\end{bmatrix}}_{\underline{\mathrm{z}}}, \quad (18)$$

where $\Phi(\mathrm{x})$ is a nonlinear vector function, u and v are the coordinates in [m] of the vehicle in a uv-plane, s is the speed of the vehicle (sometimes referred to as 'polar velocity') in [m/s], ψ is the heading angle with respect to (w.r.t.) the u-axis in [rad], θ is the heading rate in [rad/s], $\underline{z}_{\dot{\mathsf{s}}}$ is the process noise modelling the longitudinal acceleration in [m/s^2], and $\underline{z}_{\dot{\theta}}$ is the process noise modelling the heading acceleration in [rad/s^2].

We assume that $\underline{z} \in \mathbb{R}^2$ is a white-noise random process with spectral density matrix $S_{zz} = \text{diag}([q_{\dot{s}} \quad q_{\dot{\theta}}])$, where $q_{\dot{s}}$ is the spectral density in $[\text{m}^2/s^3]$ and $q_{\dot{\theta}}$ in $[\text{rad}^2/s^3]$. These assumptions are suitable for highway driving conditions [39]. The process-noise is $\underline{\text{d}} = \int_{\Delta \text{t}} e^{F(\text{t}-\tau)} G\, \underline{\text{z}}(\tau) d\tau$ and the process-noise variance-covariance matrix is given by [42]

$$Q_{\text{dd}} = \int_{\Delta \text{t}} \left(e^{F(\text{t}-\tau)} G\right) S_{zz} \left(e^{F(\text{t}-\tau)} G\right)^T d\tau, \tag{19}$$

where $\Delta \text{t} = \text{t} - \text{t}_0$ is the time update step in $[s]$, $e^{F(\text{t}-\tau)} = \sum_{j=0}^{\infty} \frac{F^j(\text{t}-\tau)^j}{j!}$, and $F = \partial_{\text{x}^T} \Phi\left(\text{x}^{(0)}\right)$ for an appropriately chosen linearization point $\text{x}^{(0)}$.

The following measurement model is considered

$$\begin{aligned} \mathsf{E}(\underline{\text{y}}^{(co)}) &= \left[\text{u}^{(1)} \quad \text{v}^{(1)} \quad \text{u}^{(2)} \quad \text{v}^{(2)} \quad l^{(12)} \quad l^{(21)}\right]^T, \\ R^{(co)} &= \text{blkdiag}\left([R_1 \quad R_2 \quad R_l]\right), \end{aligned} \tag{20}$$

where $(\text{u}^{(1)}, \text{v}^{(1)})$ is the position of vehicle 1 in [m], $(\text{u}^{(2)}, \text{v}^{(2)})$ of vehicle 2 in [m], $l^{(12)}$ and $l^{(21)}$ are the inter-vehicle distances in [m]. Then we have for $j \in \{1, 2\}$, the variance-covariance of the position measurements $R_j = \begin{bmatrix} \sigma^2_{\text{u}_j} & \rho_j \sigma_{\text{u}_j} \sigma_{\text{v}_j} \\ \rho_j \sigma_{\text{u}_j} \sigma_{\text{v}_j} & \sigma^2_{\text{v}_j} \end{bmatrix}$ $[\text{m}^2]$ and that of the distance measurements $R_l = \text{diag}\left(\begin{bmatrix} \sigma^2_{l_{12}} & \sigma^2_{l_{21}} \end{bmatrix}\right)$ $[\text{m}^2]$. Sensor calibration is presumed to ensure that all measurements are referenced to a defined Center of Reference (CoR) situated at the geometric center of the vehicle's rooftop. Since these motion and measurement models are nonlinear, we implement an EKF. The framework presented in Section II holds as it is valid for both linear and linearized models with the appropriate changes (e.g., using the jacobian $\text{J}_\Phi \in \mathbb{R}^{n \times n}$ of the vector function $\Phi(.)$ and $\text{J}_A \in \mathbb{R}^{m \times n}$ of the vector function $A(.)$) [26]. From (20) it follows that $m = 6$.

B. Alternative Hypotheses

Based on the previously discussed motion and measurement models, we formulate the following alternative hypotheses for the statistical testing procedure in which we account for:

- *Model misspecifications in motion models* $\mathcal{H}_1 : \mathsf{E}\left(\underline{\nu}\right) = \left(-\text{J}_A \text{J}_\Phi\right) C_1 b_1$ and $\mathcal{H}_2 : \mathsf{E}\left(\underline{\nu}\right) = \left(-\text{J}_A \text{J}_\Phi\right) C_2 b_2$, with $q_1 = q_2 = 1$, and $b_1, b_2 \in \mathbb{R}$ in $[\text{m}/s^2]$, account for longitudinal deceleration or acceleration of vehicles 1 and 2. These types of model misspecifications are expressed as

$$\begin{aligned} C_1 &= \begin{bmatrix} 0 & 0 & 1 & 0 & 0 & 0 & 0 & 0 & 0 & 0 \end{bmatrix}^T, \\ C_2 &= \begin{bmatrix} 0 & 0 & 0 & 0 & 0 & 0 & 0 & 1 & 0 & 0 \end{bmatrix}^T. \end{aligned} \tag{21}$$

- *Model misspecifications in position measurements* $\mathcal{H}_3 : \mathsf{E}\left(\underline{\nu}\right) = C_3 b_3$ and $\mathcal{H}_4 : \mathsf{E}\left(\underline{\nu}\right) = C_4 b_4$, with $q_3 = q_4 = 2$, and $b_3, b_4 \in \mathbb{R}^2$ in [m], account for 2D model misspecifications in the position measurements of vehicles 1 and 2 (outliers in positions). These types of model misspecifications are expressed as

$$\begin{aligned} C_3 &= \begin{bmatrix} 1 & 0 & 0 & 0 & 0 & 0 \\ 0 & 1 & 0 & 0 & 0 & 0 \end{bmatrix}^T, \\ C_4 &= \begin{bmatrix} 0 & 0 & 1 & 0 & 0 & 0 \\ 0 & 0 & 0 & 1 & 0 & 0 \end{bmatrix}^T. \end{aligned} \tag{22}$$

- *Model misspecifications in inter-vehicle distance measurements* $\mathcal{H}_5 : \mathsf{E}\left(\underline{\nu}\right) = C_5 b_5$ and $\mathcal{H}_6 : \mathsf{E}\left(\underline{\nu}\right) = C_6 b_6$, with $q_5 = q_6 = 1$, and $b_5, b_6 \in \mathbb{R}$ in [m], account for 1D model misspecifications in the inter-vehicle distance measurements. These types of model misspecifications are expressed as

$$\begin{aligned} C_5 &= \begin{bmatrix} 0 & 0 & 0 & 0 & 1 & 0 \end{bmatrix}^T, \\ C_6 &= \begin{bmatrix} 0 & 0 & 0 & 0 & 0 & 1 \end{bmatrix}^T. \end{aligned} \tag{23}$$

With the alternative hypotheses defined, the formulation of the partitions $\mathcal{P}_i \subset \mathbb{R}^m$ can carried out according to the principles in (4) and (6). The combined outcome of the EKF and of the DIA procedure for the two-car cooperative (co) positioning setting is

$$\overline{\underline{\text{x}}}^{(co)} = \begin{bmatrix} \overline{\underline{\text{x}}}^{(1)} \\ \overline{\underline{\text{x}}}^{(2)} \end{bmatrix}. \tag{24}$$

which results in the dimension $n = n_1 + n_2 = 10$. The filter error $\overline{\underline{\epsilon}}^{(co)} = \underline{\text{x}}^{(co)} - \overline{\underline{\text{x}}}^{(co)}$ and the process-noise variance-covariance matrix are expressed as

$$\overline{\underline{\epsilon}}^{(co)} = \begin{bmatrix} \overline{\underline{\epsilon}}^{(1)} \\ \overline{\underline{\epsilon}}^{(2)} \end{bmatrix}, \quad Q^{(co)}_{\text{dd}} = \text{blkdiag}\left(\begin{bmatrix} Q^{(1)}_{\text{dd}} & Q^{(2)}_{\text{dd}} \end{bmatrix}\right). \tag{25}$$

C. Scenario With a Single Configuration of the vehicles

In this simulation scenario, two vehicles are driving on a highway, on the Center of Lanes (CoL), which are parallel, and have a width (l_w) of 3.5 [m] each [43]. Both vehicles are set to have a length of 4.5 [m] and a width of 1.8 [m] [44]. The geometry of the scenario and the details of the simulation parameters are given in Figure 3 and Table II.

The spectral densities are chosen to model realistic vehicle behavior on a highway, accounting for gentle acceleration or deceleration of 0.5 $[\text{m}/s^2]$ in the longitudinal direction [46]. For smooth lateral maneuvers, such as lane changes, the spectral density corresponds to variations of 0.03 $[\text{rad}/s^2]$ (1.81 $[\text{deg}/s^2]$). The position measurements have a precision (standard deviation) of 0.100 [m], indicative of positioning via Differential GNSS (DGNSS) [47]. The precision of the inter-vehicle distance measurements (0.050 [m]) is assumed to rely on an automotive-grade LiDAR system.

Our analysis focuses on vehicle 1, though a similar approach is applicable to vehicle 2. Therefore we are interested only in the filter error of the 2D position of vehicle 1 (at a single-epoch), $\overline{\underline{\varepsilon}} = H^T \overline{\underline{\epsilon}}^{(co)}$, with $H^T = \begin{bmatrix} I_2 & 0_{2\times 8} \end{bmatrix}$ (we omit the index 1 for simplicity). The PDF of $\overline{\underline{\varepsilon}}$ is

$$f_{\overline{\underline{\varepsilon}}}(\varepsilon) = \sum_{i=0}^{n_\mathcal{H}} \int_{\mathcal{P}_i} f_{\hat{\underline{\varepsilon}}_0}\left(\varepsilon + H^T L_i \upsilon\right) f_{\underline{\nu}}(\upsilon) d\upsilon, \tag{26}$$

and the results from Section III follow similarly.

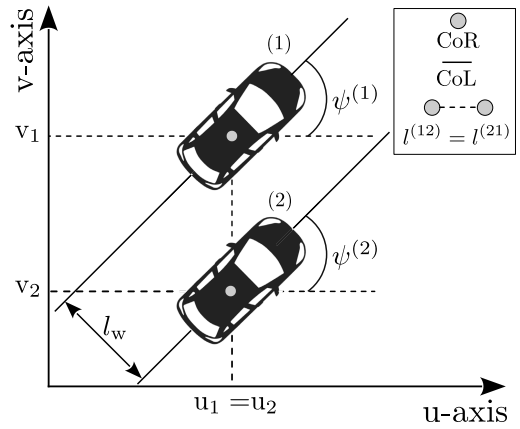

Fig. 3. Schematic representation of the 2D geometry for the single configuration simulation scenario. Source: Adapted from [45].

TABLE II
SIMULATION PARAMETERS AND THEIR VALUES

Parameter(s)	Value	Details
$s^{(j)}$	28 [m/s] (≈101 [km/h])	$j = \{1, 2\}$
$\psi^{(j)}$	45 [deg]	
$q_{\dot{\xi}}^{(j)}$	0.250 [m^2/s^3]	
$q_{\dot{\theta}}^{(j)}$	0.001 [rad^2/s^3]	
σ_{u_j}, σ_{v_j}	0.100 [m]	
ρ_j	0.200	
$\sigma_{l_{12}}$, $\sigma_{l_{21}}$	0.050 [m]	-
$l^{(12)}$, $l^{(21)}$	4.950 [m]	$\sqrt{2}\, l_w$
Δt	1 [s]	time update step

Established requirements for the shape and size of the safety-region $\mathcal{B}$ are not yet formalized for positioning of automated/autonomous vehicles. However, some research studies are available in which rectangular and elliptical shapes have been used [5], [48], [49]. For our analysis we choose an ellipse to inscribe the shape of the vehicle. The safety region is defined as

$$\mathcal{B} = \left\{ \varepsilon \in \mathbb{R}^2 |\ ||\varepsilon||^2_{Q_\mathcal{B}} \leq 1 \right\}, \tag{27}$$

where $Q_\mathcal{B}^{-1} = \begin{bmatrix} 0.358 & -0.259 \\ -0.259 & 0.358 \end{bmatrix}$ [m^{-2}]. The major-axis of $\mathcal{B}$ has a length of 6.36 [m] with an orientation w.r.t. the horizontal axis of 45°, and the minor-axis has a length of 2.55 [m]. In the next subsections (IV-C.1 and IV-C.2) we present an analysis of the components of the PDFs of $\underline{\bar{\varepsilon}}$ under $\mathcal{H}_0$ and $\mathcal{H}_{i\neq 0}$. In the last subsection (IV-C.3), the resulting probability of positioning failure is discussed, comparing the cases where the dependence between parameter estimation and statistical hypothesis testing is accounted for and when it is ignored.

1) Components of $f_{\underline{\bar{\varepsilon}}}(\varepsilon|\mathcal{H}_0)$: The components of $f_{\underline{\bar{\varepsilon}}}(\varepsilon|\mathcal{H}_0)$ are shown in Figure 4. Since in $\mathbb{R}^m$ there is a symmetry of $f_{\underline{\nu}}(\nu|\mathcal{H}_0)$ about the origin and the partitions $\mathcal{P}_i$, it follows that $\mathsf{E}\left(\underline{\bar{\varepsilon}}|\mathcal{H}_0\right) = 0_{n_1\times 1}$. Under the events of FA$_i$'s, the orientation, shape, size, and multimodality are an outcome of the averaged shifted functions $f_{\underline{\hat{\varepsilon}}_0}\left(\varepsilon + H^T L_i\, \nu|\mathcal{H}_0\right)$ for $\underline{\nu} \in \mathcal{P}_i$ (the outcome of statistical testing). The study of the variability of the shifting term $H^T L_i\, \underline{\nu}$ will give an indication of the amount of variability under $\mathcal{H}_{i\neq 0}$, while $\mathcal{H}_0$ is valid. Therefore we do an analysis of the ellipses spanned by $\zeta^T Q_i^{-1} \zeta = 1$, with $\zeta \in \mathbb{R}^2$, $Q_i^{-1} = \left[\left(H^T L_i\right) Q_{\nu\nu} \left(L_i^T H\right)\right]^{-1}$ which can be factorized as $Q_i^{-1} = U_i \Lambda_i U_i^T$ (based on the eigendecomposition). Table III shows the eigenvalues of each Q_i^{-1}, the length of the principal axis (p.a.), and the angle ($\measuredangle$) of the p.a.'s w.r.t. the u-axis (measured counterclockwise).

TABLE III
EIGENVALUES, LENGTH OF P.A., AND $\measuredangle$ OF P.A. W.R.T. U-AXIS

Q_i^{-1}	Eigenvalues [m^{-2}]	Length of p.a. [m]	$\measuredangle$ [deg]
1	$(4.17 \cdot 10^3,\ 0)$	$1.55 \cdot 10^{-2}$	30.03
2	$(0,\ 2.06 \cdot 10^4)$	$6.97 \cdot 10^{-3}$	80.18
3	$(0.26 \cdot 10^1,\ 1.81 \cdot 10^2)$	$1.96 \cdot 10^{-1}$	178.71
4	$(5.33 \cdot 10^7,\ 2.21 \cdot 10^2)$	$6.73 \cdot 10^{-2}$	78.77
5	$(0,\ 3.72 \cdot 10^3)$	$1.64 \cdot 10^{-2}$	78.79
6	$(0,\ 3.72 \cdot 10^3)$	$1.64 \cdot 10^{-2}$	78.79

Since the hypotheses $\mathcal{H}_i$ model 1D model misspecifications for $i \in \{1, 2, 5, 6\}$, it means that through the corresponding L_i terms, the obtained Q_i^{-1} matrices have only one nonzero eigenvalue. Although $\mathcal{H}_1$ models a model misspecification in the longitudinal speed of vehicle 1, the orientation of the p.a. of Q_1^{-1} is driven by the direction of motion of vehicle 1 and by the correlation between the position states of the two vehicles due to the distance measurements. The correlation depends on the relative position of vehicle 2 w.r.t. vehicle 1, and on the structure in (20). As the CoR of vehicle 2 has almost the same u-coordinates as of vehicle 1, the aforementioned (inter-vehicle) correlation will 'pull' the p.a. of Q_1^{-1} from an angle of 45 [deg] to one of 30.03 [deg]. The direction of the p.a. of Q_2^{-1} is tilted more towards the v-axis, the main contributor being the relative position of the vehicles (captured by the inter-vehicle correlation). The p.a.'s of Q_5^{-1} and Q_6^{-1} are also tilted more towards the v-axis due to the inter-vehicle correlation.

The parameters of the ellipses corresponding to Q_5^{-1} and Q_6^{-1} are the same since the corresponding entries in the design matrix and the precision of the distance measurements, for both ways, are the same. The conditional PDFs $f_{\underline{\bar{\varepsilon}}|\text{FA}_i}(\varepsilon|\text{FA}_i)$ for $i \in \{1, 2, 5, 6\}$ do not exhibit multimodality as the outcome of statistical testing reveals that $H^T L_i\, \underline{\nu}$ with $\underline{\nu} \in \mathcal{P}_i$ is closely distributed across the p.a. The impact of falsely accepting $\mathcal{H}_1$, $\mathcal{H}_2$, $\mathcal{H}_5$ or $\mathcal{H}_6$, while $\mathcal{H}_0$ is valid, on the positioning safety of vehicle 1 is not expected to be significant (see Figure 4).

As the hypotheses $\mathcal{H}_3$ and $\mathcal{H}_4$ model 2D model misspecifications in the position measurements of vehicle 1 and vehicle 2, the matrices Q_3^{-1} and Q_4^{-1} have two nonzero eigenvalues. The eigenvalues and the orientation of the p.a. of Q_3^{-1} indicate a larger variation along the u-axis than along the v-axis. The variation is smaller on the v-axis due contribution of the [cm]-level inter-vehicle distance measurements and due to the relative position of vehicle 2 w.r.t. vehicle 1. The large variation along the u-axis is captured by the length of the p.a. and its explanation can be given by investigating the components of

$$Q_3^{-1} = \left[\left(H^T L_3\right) R \left(L_3^T H\right) + \left(H^T L_3\right) \mathrm{J}_A P^- \mathrm{J}_A^T \left(L_3^T H\right)\right]^{-1}. \tag{28}$$

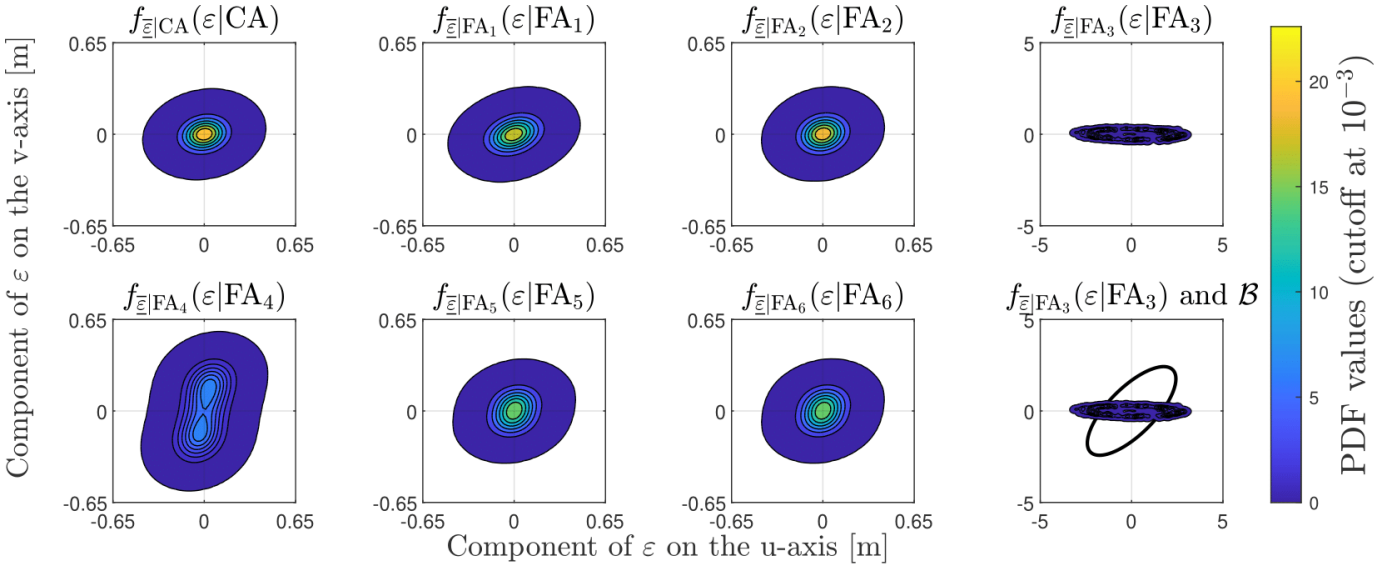

Fig. 4. Components of $f_{\underline{\varepsilon}}(\varepsilon|\mathcal{H}_0)$ for $\alpha = 10^{-3}$ and $n_\nu = 10^6$ pseudo-random samples drawn from $f_{\underline{\nu}}(\nu|\mathcal{H}_0)$ (note the different scale of $f_{\underline{\varepsilon}|\mathrm{FA}_3}(\varepsilon|\mathrm{FA}_3)$). The last figure in the second row is $f_{\underline{\varepsilon}|\mathrm{FA}_3}(\varepsilon|\mathrm{FA}_3)$ in relation with the safety region $\mathcal{B}$.

The second term in (28) is dominant through the contribution of the process-noise variance-covariance matrix Q_{dd} (see also Table II). Despite the [dm]-level position measurements and [cm]-level inter-vehicle distance measurements, the considered variations in longitudinal acceleration and in heading acceleration are the driving factors. At the bottom right of Figure 4 the component $f_{\underline{\varepsilon}|\mathrm{FA}_3}(\varepsilon|\mathrm{FA}_3)$ is displayed in relation with the safety region $\mathcal{B}$, which indicates that it has the largest probability density outside $\mathcal{B}$ among all components of $f_{\underline{\varepsilon}}(\varepsilon|\mathcal{H}_0)$. Although the term $H^T L_3 \underline{\nu}$ with $\underline{\nu} \in \mathcal{P}_3$ is sparsely distributed, it manifests a 'smearing' effect by $f_{\underline{\hat{\varepsilon}}_0}\left(\varepsilon + H^T L_3 \nu|\mathcal{H}_0\right)$ instead of a multimodality. The 'smearing' is related to the elongation of Q_3^{-1} in the 2D space (a condition number of 2.638). In the case of Q_4^{-1}, the largest variation is along the v-axis as the direction of the p.a. is driven by the inter-vehicle correlation and their relative positions. Since the ellipse is highly elongated along the p.a. (a condition number of $4.91 \cdot 10^2$), which also has the second largest length, the sparsely distributed $H^T L_4 \underline{\nu}$ with $\underline{\nu} \in \mathcal{P}_4$ is causing $f_{\underline{\varepsilon}|\mathrm{FA}_4}(\varepsilon|\mathrm{FA}_4)$ to be bimodal.

2) Components of $f_{\underline{\varepsilon}}(\varepsilon|\mathcal{H}_1)$: Since under any $\mathcal{H}_{i\neq 0}$ the PDF of $\underline{\varepsilon}$ depends on the b_i's (see (12)), one needs to choose or make assumptions on the size of the model misspecification. We show the analysis of the components of $f_{\underline{\varepsilon}}(\varepsilon|\mathcal{H}_1)$, though similarly this can be done for the other hypotheses. Under $\mathcal{H}_1$ we assume a model misspecification of $b_1 = -3$ [m/s^2] (a longitudinal deceleration). This case corresponds to a braking event done by vehicle 1 (e.g., due to a congestion on the lane). In this case there is no symmetry of $f_{\underline{\nu}}(\nu|\mathcal{H}_1)$ about the origin and the partitions $\mathcal{P}_i$ (this is true for any $\mathcal{H}_{i\neq 0}$). The simulated probabilities of the decision events are shown in Figure 5.

The variability of the probabilities across the simulations in Figure 5 is higher for the lower ones given the same number of used pseudo-random samples, in this case $n_\nu = 10^6$.

An indicator for the separability between the probabilities of the events of MD_1, CI_1, and WI_i (for $i \notin \{0, 1\}$) is

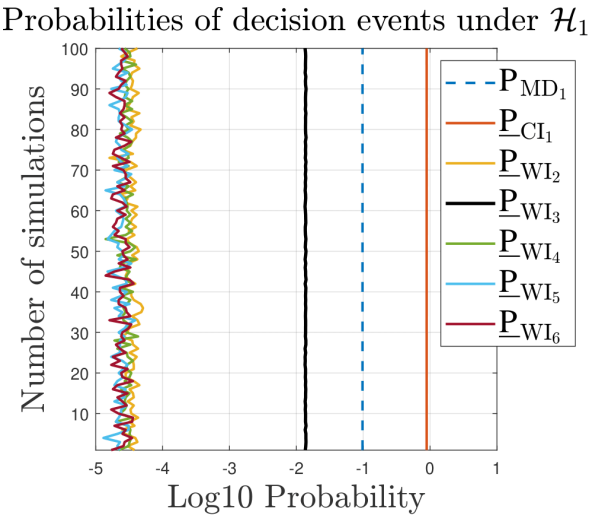

Fig. 5. The probabilities of MD_1, CI_1, and WI_i (for $i \notin \{0, 1\}$) over 100 simulations with $n_\nu = 10^6$, $\alpha = 10^{-3}$, and $b_1 = -3$ [m/s^2].

represented by the angles between the subpaces of $\mathbb{R}^m$ spanned by $\mathcal{R}\left(C_1^*\right)$, $\mathcal{R}\left(C_2^*\right)$, and $\mathcal{R}\left(C_i\right)$, for $i \notin \{0, 1, 2\}$. The angles between a one-dimensional subspace and a higher-dimensional subspace in $\mathbb{R}^m$ can be computed in two steps: (i) project the one-dimensional subspace onto the higher-dimensional subspace, (ii) compute the angle between the one-dimensional subspace and the projection. When comparing subspaces in $\mathbb{R}^m$, each with a dimension larger than one, the concept of canonical (or principal angles) is used [50], [51], [52]. The inner products involved in the computation of the angles are with respect to the metric defined by $Q_{\nu\nu}^{-1}$ (Algorithm 6.1 of [52]). The obtained angles are presented in Table IV.

Table IV shows that the angle $\measuredangle\left(\mathcal{R}\left(C_1^*\right), \mathcal{R}\left(C_3\right)\right) = 38.13°$ is by far the smallest which means that as $f_{\underline{\nu}}(\nu|\mathcal{H}_1)$ moves along $\mathcal{R}\left(C_1^*\right)$ in $\mathcal{P}_1$, the probability density outside $\mathcal{P}_1$ will be larger in $\mathcal{P}_3$ than in $\mathcal{P}_2$, $\mathcal{P}_4$, $\mathcal{P}_5$, or $\mathcal{P}_6$. This is

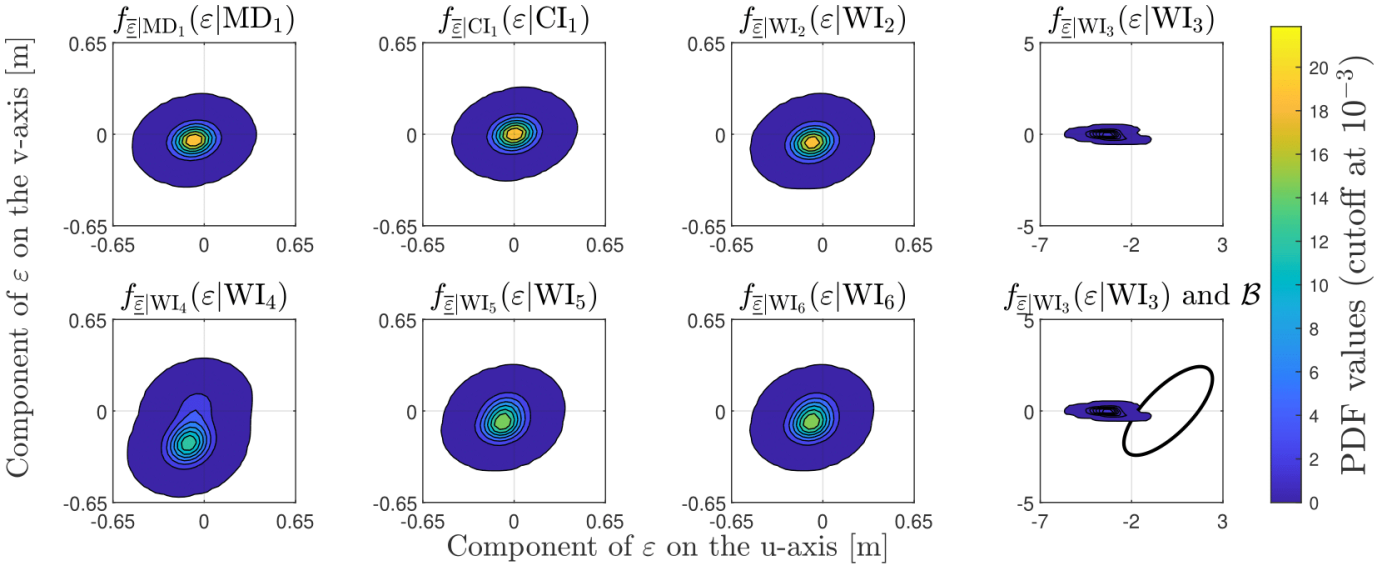

Fig. 6. Components of $f_{\underline{\varepsilon}}(\varepsilon|\mathcal{H}_1)$ for $\alpha = 10^{-3}$, $b_1 = -3$ [m/s^2], and $n_\nu = 10^6$ pseudo-random samples drawn from $f_{\underline{\nu}}(\nu|\mathcal{H}_1)$ (note the different scale of $f_{\underline{\varepsilon}|\mathrm{WI}_3}(\varepsilon|\mathrm{WI}_3)$). The last figure from the second-column is $f_{\underline{\varepsilon}|\mathrm{WI}_3}(\varepsilon|\mathrm{WI}_3)$ in relation with the safety region $\mathcal{B}$.

TABLE IV
ANGLES BETWEEN $\mathcal{R}(C_1^*)$ AND $\mathcal{R}(C_2^*)$, $\mathcal{R}(C_i)$ FOR $i \notin \{0, 1, 2\}$

Subspace	$\mathcal{R}(C_2^*)$	$\mathcal{R}(C_3)$	$\mathcal{R}(C_4)$	$\mathcal{R}(C_5)$	$\mathcal{R}(C_6)$
$\mathcal{R}(C_1^*)$	85.98°	38.13°	84.22°	88.34°	88.34°

confirmed by Figure 5 which shows that, among the wrong identifications, $\mathsf{P}_{\mathrm{WI}_3}$ is largest with a mean value of $0.137 \cdot 10^{-1} \pm 1.177 \cdot 10^{-5}$ (over 100 simulations). In practice this means that in the case of a moderate to hard braking event by vehicle 1, the probability to wrongly identify $\mathcal{H}_3$, when $\mathcal{H}_1$ is valid, is significantly larger than any of the other probabilities of wrong identification. With respect to the components of $f_{\underline{\varepsilon}}(\varepsilon|\mathcal{H}_1)$ we observe that $f_{\underline{\varepsilon}|\mathrm{WI}_3}(\varepsilon|\mathrm{WI}_3)$ is the most shifted away from the origin (see Figure 6).

In the case of an alternative hypothesis such as $\mathcal{H}_1$, the shape of the conditional PDFs is also driven by the model misspecification. The term $H^T L_i \underline{\nu}$ with $\underline{\nu} \in \mathcal{P}_i$ and $\underline{\nu} \sim f_{\underline{\nu}}(\nu|\mathcal{H}_1)$ is distributed and shifted along the subspaces of $\mathbb{R}^2$ spanned by $\mathcal{R}(H^T L_i C_1^*)$ for $i \in \{1, \ldots, 6\}$. This in turn impacts the modes of the conditional PDFs as a result of the averaging of the shifted functions $f_{\hat{\underline{\varepsilon}}_0}(\varepsilon + H^T L_i \nu|\mathcal{H}_1)$ according to (26). As Figure 6 shows, the impact of wrongly identifying $\mathcal{H}_3$, while $\mathcal{H}_1$ is valid, on the positioning safety of vehicle 1 will be largest. A similar analysis for the other $f_{\underline{\varepsilon}}(\varepsilon|\mathcal{H}_i)$ when $i \in \{2, 4, 5, 6\}$ reveals that the positioning safety of vehicle 1 is also impacted most by the component corresponding to the wrong identification of $\mathcal{H}_3$. In the case of $f_{\underline{\varepsilon}}(\varepsilon|\mathcal{H}_3)$, the conditional component $f_{\underline{\varepsilon}|\mathrm{MD}_3}(\varepsilon|\mathrm{MD}_3)$ has the largest impact.

3) Total Probability of Positioning Failure: The total probability of positioning failure $\mathbb{P}_{\mathcal{F}}(\mathsf{b})$ from (15) depends on $\mathsf{b} = \{b_1, b_2, \ldots, b_{n_\mathcal{H}}\}$. By evaluating $\mathbb{P}_{\mathcal{F}}(\mathsf{b})$ over ranges of the model misspecifications one can obtain the worst-case scenario.

First, we show the results of the computations for $\mathbb{P}_{\mathcal{F}}|\mathcal{H}_0$ and for the maximum $\mathbb{P}_{\mathcal{F}}|\mathcal{H}_i$ for $i \in \{1, \ldots, n_\mathcal{H}\}$ in Table V over 100 simulations together with the determined Most Influential Component (MIC). We define the MIC to be the component of a $\mathbb{P}_{\mathcal{F}}|\mathcal{H}_i$ which has the largest contribution, or is the most influential ($\mathrm{MIC}_\mathrm{E} = \mathsf{P}_\mathrm{E}\,\mathbb{P}_{\mathcal{F}}|\mathrm{E}$). The MICs are also useful to compare the safety-performance of different statistical hypothesis testing strategies (i.e., different choices of partitioning of $\mathbb{R}^m$).

TABLE V
COMPUTED MAXIMUM PROBABILITIES OF POSITIONING FAILURE OVER 100 SIMULATIONS (μ_SIM AND σ_SIM), WORST-CASE BIASES PER $\mathcal{H}_i$ FOR $i \in \{1, \ldots, n_\mathcal{H}\}$, AND MICS

Comp.	μ_sim	σ_sim	b [unit]	MIC
$\mathbb{P}_{\mathcal{F}}|\mathcal{H}_0$	$1.3 \cdot 10^{-4}$	$8.3 \cdot 10^{-7}$	-	$\mathrm{MIC}_{\mathrm{FA}_3}$
$\mathbb{P}_{\mathcal{F}}|\mathcal{H}_1$	$1.9 \cdot 10^{-2}$	$1.1 \cdot 10^{-4}$	± 2.2 [m/s^2]	$\mathrm{MIC}_{\mathrm{WI}_3}$
$\mathbb{P}_{\mathcal{F}}|\mathcal{H}_2$	$4.1 \cdot 10^{-4}$	$3.7 \cdot 10^{-6}$	± 1.5 [m/s^2]	$\mathrm{MIC}_{\mathrm{WI}_3}$
$\mathbb{P}_{\mathcal{F}}|\mathcal{H}_3$	$8.3 \cdot 10^{-1}$	$3.4 \cdot 10^{-3}$	$\pm[2.1\ 0.0]^T$ [m]	$\mathrm{MIC}_{\mathrm{MD}_3}$
$\mathbb{P}_{\mathcal{F}}|\mathcal{H}_4$	$4.8 \cdot 10^{-2}$	$1.5 \cdot 10^{-4}$	$\pm[0.3\ -0.9]^T$ [m]	$\mathrm{MIC}_{\mathrm{WI}_3}$
$\mathbb{P}_{\mathcal{F}}|\mathcal{H}_5$	$4.9 \cdot 10^{-4}$	$4.5 \cdot 10^{-6}$	± 0.2 [m]	$\mathrm{MIC}_{\mathrm{WI}_3}$
$\mathbb{P}_{\mathcal{F}}|\mathcal{H}_6$	$4.9 \cdot 10^{-4}$	$4.7 \cdot 10^{-6}$	± 0.2 [m]	$\mathrm{MIC}_{\mathrm{WI}_3}$

In the case of $\underline{\mathbb{P}}_{\mathcal{F}}|\mathcal{H}_0$ the mean value of $1.3 \cdot 10^{-4} \pm 8.3 \cdot 10^{-7}$ is rather high considering [dm]-level positioning measurement and [cm]-level inter-vehicle distance measurements. The MIC of $\underline{\mathbb{P}}_{\mathcal{F}}|\mathcal{H}_0$ is

$$\mathrm{MIC}_{\mathrm{FA}_3} = \mathsf{P}_{\mathrm{FA}_3}\left(\int_{\mathcal{B}^c} f_{\underline{\varepsilon}|\mathrm{FA}_3}(\varepsilon|\mathrm{FA}_3)\, d\varepsilon\right) \tag{29}$$

with $f_{\underline{\varepsilon}|\mathrm{FA}_3}(\varepsilon|\mathrm{FA}_3) = \frac{\int_{\mathcal{P}_3} f_{\hat{\underline{\varepsilon}}_0}(\varepsilon + H^T L_3 \upsilon|\mathcal{H}_0)\, f_{\underline{\nu}}(\upsilon|\mathcal{H}_0) d\upsilon}{\mathsf{P}_{\mathrm{FA}_3}}$ having the most probability density outside $\mathcal{B}$ across all of the components. This confirms the analysis done based on Figure 4 and of $Q_3^{-1} = \left[\left(H^T L_3\right) Q_{\nu\nu} \left(L_3^T H\right)\right]^{-1}$ from Table III and (28). Under $\mathcal{H}_3$, in the case of model misspecifications in the GNSS-based position measurements at [m]-level ($\pm[2.1\ 0.0]^T$ [m]) for vehicle 1, the maximum of the mean value of

TABLE VI
VERIFICATION OF RESULTS IN TABLE V VIA STANDARD MONTE CARLO OVER 100 SIMULATIONS (μ_{SIM} AND σ_{SIM})

Comp.	μ_{sim}	σ_{sim}	b [unit]
$\underline{\mathbb{P}}_{\mathcal{F}}\|\mathcal{H}_0$	$1.3 \cdot 10^{-4}$	$3.4 \cdot 10^{-6}$	-
$\underline{\mathbb{P}}_{\mathcal{F}}\|\mathcal{H}_1$	$1.9 \cdot 10^{-2}$	$4.1 \cdot 10^{-5}$	-2.2 [m/s^2]
$\underline{\mathbb{P}}_{\mathcal{F}}\|\mathcal{H}_2$	$4.2 \cdot 10^{-4}$	$6.9 \cdot 10^{-6}$	± 1.5 [m/s^2]
$\underline{\mathbb{P}}_{\mathcal{F}}\|\mathcal{H}_3$	$8.3 \cdot 10^{-1}$	$1.2 \cdot 10^{-4}$	$\pm$[-2.1 0.0]^T[m]
$\underline{\mathbb{P}}_{\mathcal{F}}\|\mathcal{H}_4$	$4.8 \cdot 10^{-2}$	$6.4 \cdot 10^{-5}$	$\pm$[0.3 -0.9]^T[m]
$\underline{\mathbb{P}}_{\mathcal{F}}\|\mathcal{H}_5$	$4.9 \cdot 10^{-4}$	$6.3 \cdot 10^{-6}$	± 0.2 [m]
$\underline{\mathbb{P}}_{\mathcal{F}}\|\mathcal{H}_6$	$4.9 \cdot 10^{-4}$	$6.9 \cdot 10^{-6}$	± 0.2 [m]

$\underline{\mathbb{P}}_{\mathcal{F}}|\mathcal{H}_3$ is $8.3 \cdot 10^{-1} \pm 3.4 \cdot 10^{-3}$, which is also the largest across all components from Table V. The result is expected since, among all alternative hypotheses $\mathcal{H}_{i \neq 0}$ considered, alternative hypothesis $\mathcal{H}_3$ specifically addresses model misspecifications in the position measurements of vehicle 1.

Once the maximum $\underline{\mathbb{P}}_{\mathcal{F}}|\mathcal{H}_i$ for $i \in \{1, \ldots, n_{\mathcal{H}}\}$ are determined, the next step is to compute the worst-case total probability of positioning failure based on (15), in which the weights $\omega_i = \mathsf{P}(\mathcal{H}_i)$ have to be set. In line with the EKF update step of $\Delta t = 1$ [s], the a-priori $\mathsf{P}(\mathcal{H}_i)$ are chosen on a per second basis. The chosen values serve as examples based on several studies and existing standards: (i) $\mathsf{P}(\mathcal{H}_1) = \mathsf{P}(\mathcal{H}_2) = 10^{-6}$ which corresponds to harsh vehicle braking events while driving on highways [53], (ii) $\mathsf{P}(\mathcal{H}_3) = \mathsf{P}(\mathcal{H}_4) = 10^{-5}$ corresponds to a position error potentially due to a fault in the signal-in-space of a GNSS (e.g., GPS) satellite [54], (iii) $\mathsf{P}(\mathcal{H}_5) = \mathsf{P}(\mathcal{H}_6) = 10^{-5}$ represents an example of a probability of failure of the LiDAR according to a study in [55], and (iv) $\mathsf{P}(\mathcal{H}_0) = 1 - \sum_{i=1}^{n_{\mathcal{H}}} \mathsf{P}(\mathcal{H}_i) = 9.9996 \cdot 10^{-1}$. Using these assumptions and the results from Table V, the worst-case scenario total probability of positioning failure is computed to be

$$\underline{\mathbb{P}}_{\mathcal{F}}(\mathsf{b}) = 1.4 \cdot 10^{-4} \pm 8.3 \cdot 10^{-7}. \tag{30}$$

In the case that safety requirements are established, (30) can be used to determine whether the requirements are met.

If, in the safety-analysis, one would *ignore* the dependence between parameter estimation and statistical hypothesis testing then the worst-case scenario total probability of positioning failure would be based on (16) and (17), which gives

$$\underline{\mathbb{P}}^{o}_{\mathcal{F}}(\mathsf{b}) = 1.2 \cdot 10^{-5} \pm 4.5 \cdot 10^{-8}. \tag{31}$$

We notice that $\underline{\mathbb{P}}^{o}_{\mathcal{F}}(\mathsf{b})$ is lower than $\underline{\mathbb{P}}_{\mathcal{F}}(\mathsf{b})$ from (30) by approximately *an order of magnitude* (i.e., it provides a too optimistic assessment).

4) Verification of Results: To verify the results from Table V we use a 'crude' Monte Carlo simulation to generate $n_\varepsilon = 10^5$ pseudo-random samples $\bar{\varepsilon}$ from $f_{\bar{\varepsilon}}(\varepsilon|\mathcal{H}_i)$ for $i \in \{0, \ldots, n_{\mathcal{H}}\}$. This approach corresponds to the simulation of the EKF and the DIA procedure a chosen number of times (in this case 100) for each hypothesis. Doing so, the probabilities of positioning failure can be computed for the worst-case scenario. The obtained results are shown in Table VI.

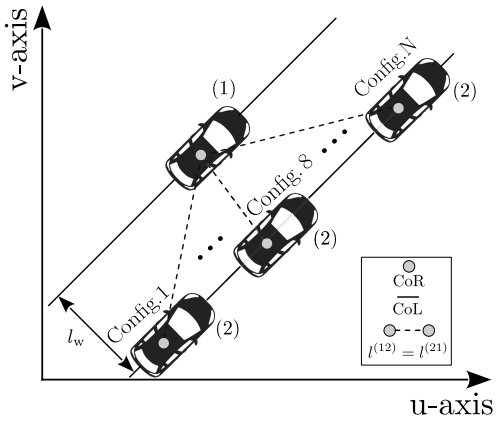

Fig. 7. Schematic representation of the 2D geometry for the multiple configuration simulation scenario simulation scenario. Source: Adapted from [45].

Next, the worst-case scenario total probability of failure is computed

$$\underline{\mathbb{P}}^{\text{MC}}_{\mathcal{F}}(\mathsf{b}) = 1.4 \cdot 10^{-4} \pm 3.4 \cdot 10^{-6}. \tag{32}$$

The results from Table VI and (32) agree with those from Table V and (30) as the relative differences are below 3%.

D. Scenario With Multiple Configurations of the Vehicles

In this simulation scenario, we study 14 distinct configurations of the two vehicles using the same simulation parameters from Table II and the previous a-priori probabilities of the hypotheses. Figure 7 provides a schematic representation of the configurations considered between vehicles 1 and 2. In these configurations, vehicle 2 is positioned at 14 equally spaced points along the center of its lane. For instance, in configuration 8, vehicle 2 is placed nearly parallel to vehicle 1. Figure 8(a) presents the results of the worst-case probabilities of positioning failure, comparing the scenarios where the dependence between parameter estimation and statistical hypothesis testing is accounted for (blue) and where it is not (red). When vehicle 2 is positioned in its own lane, either behind or in front of vehicle 1, the worst-case $\underline{\mathbb{P}}_{\mathcal{F}}(\mathsf{b})$ is highest. This is because the conditional density $f_{\bar{\varepsilon}|\text{FA}_3}(\varepsilon|\text{FA}_3)$ becomes the main contributor. Figure 8(b) illustrates that for configurations 1, 10, and 14, the conditional density $f_{\bar{\varepsilon}|\text{FA}_3}(\varepsilon|\text{FA}_3)$ has a large probability density outside the safety-region $\mathcal{B}$. In contrast for configuration 8, when the two vehicles are nearly parallel, most of the probability density lies within $\mathcal{B}$.

The over-optimism resulting from ignoring the dependence between parameter estimation and statistical hypothesis testing is quantified in Figure 9 as the ratio of the worst-case results shown in blue and red in Figure 8(a). We observe that the ratio is large when vehicle 2 is positioned in its own lane, either behind or in front of vehicle 1. However, the ratio approaches 1 when the vehicles are nearly parallel.

Thus, ignoring the aforementioned dependence leads to an overly optimistic assessment, by an order of magnitude, of the

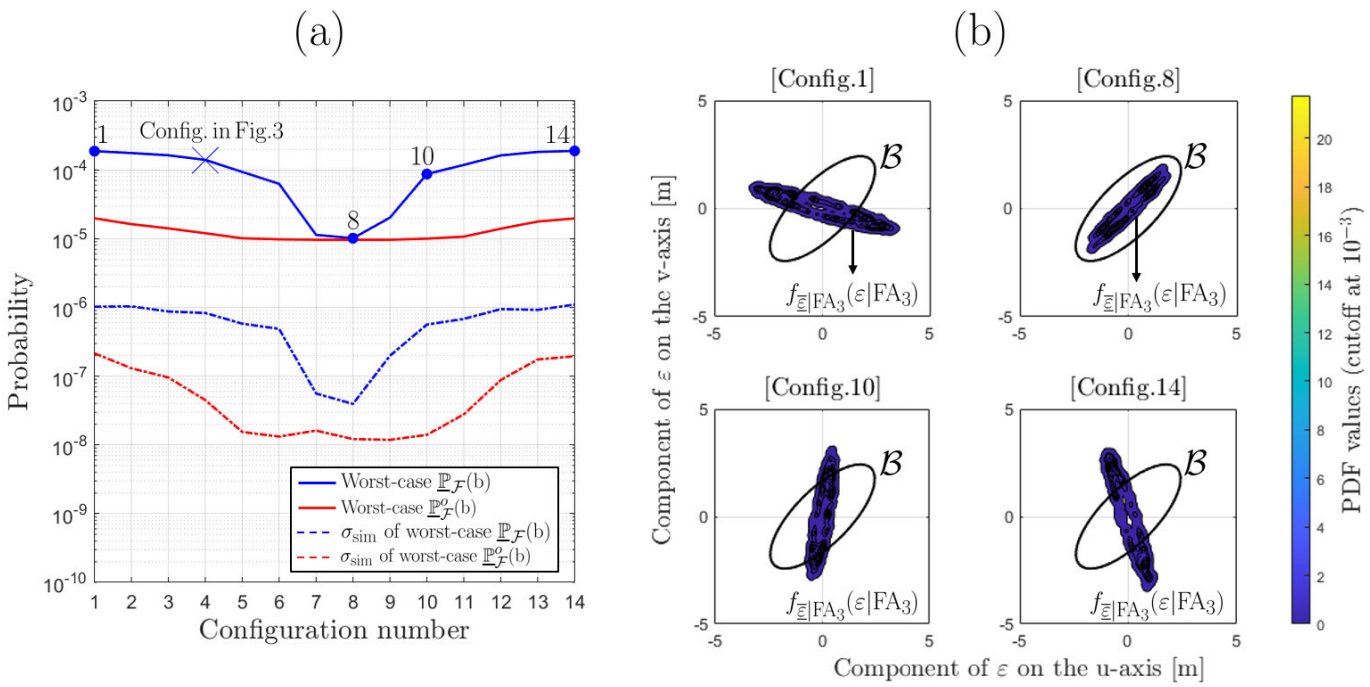

Fig. 8. (a) Worst-case probabilities of positioning failure, and their simulation standard deviations, for the 14 configurations, showing the cases where the dependence between parameter estimations is considered (blue) and ignored (red); (b) Conditional PDF $f_{\overline{\varepsilon}|\text{FA}_3}(\varepsilon|\text{FA}_3)$ in relation to the safety region $\mathcal{B}$ of vehicle 1 for configurations 1, 8, 10 and 14.

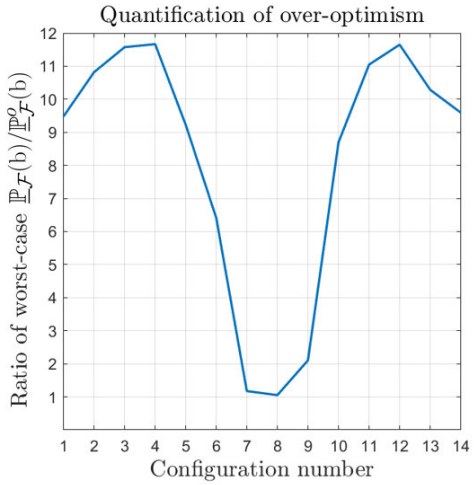

Fig. 9. Ratio of the worst-case $\underline{\mathbb{P}}_{\mathcal{F}}(\mathsf{b})/\underline{\mathbb{P}}^{o}_{\mathcal{F}}(\mathsf{b})$ to quantify the over-optimism caused by ignoring the dependence between parameter estimation and statistical hypothesis testing.

worst-case total probability of positioning failure in most of the two-vehicle configurations shown in this scenario. This could result in wrongful positioning safety assessments, such as concluding that safety requirements or guidelines are met when they are not.

E. Computational Resources

The computations were carried out on a Dell Latitude 7440 laptop, equipped with a 13th Gen Intel Core i7 processor with 10 physical cores and 16 GB of RAM. The system runs Windows 10 Enterprise, and the programming environment is MATLAB 2024a with the Parallel Computing Toolbox. The analyses utilized 10 physical cores of the processor, taking advantage of MATLAB's parallel computing capabilities. As an example, the computation time to obtain $\underline{\mathbb{P}}_{\mathcal{F}}|\mathcal{H}_0$ from Table V over 100 simulation repetitions for uncertainty quantification, was $\approx$ 5 minutes. Similarly, computing $\underline{\mathbb{P}}_{\mathcal{F}}|\mathcal{H}_i$ for a size of model missepecification was $\approx$ 5 to 7 minutes. These computation times could be reduced with access to more physical cores or by decreasing the number of independent simulation repetitions. They also depend on the programming language and code implementation. The results shown in Figure 8(a) were generated using computational resources from the Delft High Performance Computing Centre (DHPC) [56].

V. Summary and Conclusions

This contribution addressed the dependence between parameter estimation and statistical hypothesis testing in automated/autonomous vehicle positioning safety analysis and quantified the consequences of neglecting this dependence. The positioning safety discussed in this article focuses on the design stage of positioning system (i.e., offline). At this stage, key decisions are made regarding (i) measurement models, (ii) parameter estimation methods, (iii) statistical hypothesis testing procedures to account for model misspecifications (e.g., mismodeling of vehicle motion, outliers, or sensor measurement faults), and (iv) positioning scenarios for vehicles, among other factors. This approach aligns with the scenario-based safety assessment framework used for automated and autonomous vehicles [28], [29], [30]. Firstly, we have based the positioning safety analysis on the distributional theory for the DIA method which gave access

to the PDFs conditioned on the statistical hypothesis testing decision outcomes [14]. Using these conditional PDFs, the probability of positioning failure was computed for a chosen safety region $\mathcal{B}$. The expression of the total probability of positioning failure considering a set of model misspecifications $\mathsf{b} = \{b_1, b_2, \ldots, b_{n_\mathcal{H}}\}$ is,

$$\mathbb{P}_\mathcal{F}(\mathsf{b}) = \sum_{a=0}^{n_\mathcal{H}} \omega_a \int_{\mathcal{B}^c} f_{\underline{\varepsilon}}(e|\mathcal{H}_a)\, de, \tag{33}$$

with

$$\begin{aligned} f_{\underline{\varepsilon}}(\varepsilon|\mathcal{H}_a) &= \sum_{i=0}^{n_\mathcal{H}} \int_{\mathcal{P}_i} f_{\underline{\hat{\epsilon}}_i,\underline{\upsilon}}(\varepsilon, \upsilon|\mathcal{H}_a) d\upsilon \\ &= \sum_{i=0}^{n_\mathcal{H}} \int_{\mathcal{P}_i} f_{\underline{\hat{\epsilon}}_0}\left(\varepsilon + H^T L_i \upsilon|\mathcal{H}_a\right) f_{\underline{\upsilon}}(\upsilon|\mathcal{H}_a) d\upsilon, \end{aligned} \tag{34}$$

where, in the case of $i = 0$, use has been made of the independence between the normally distributed $\underline{\hat{\epsilon}}_0$ and $\underline{\upsilon}$ [38]. It is important to note that $\underline{\hat{\epsilon}}_i$ and $\underline{\upsilon}$ are *dependent* since $f_{\underline{\hat{\epsilon}}_i,\underline{\upsilon}}(\epsilon, \upsilon) \neq f_{\underline{\hat{\epsilon}}_i}(\epsilon) f_{\underline{\upsilon}}(\upsilon)$ for $i \in \{1, \ldots, n_\mathcal{H}\}$ [14].

Using, as an example, a simulation scenario of two connected vehicles driving on a highway in a cooperative positioning setting, we have accounted in the motion model of the EKF (the CTRV model), for: (i) gentle acceleration or deceleration by setting the spectral density $q_{\ddot{\mathsf{s}}}^{(j)} = 0.250$ [m$^2/s^3$] corresponding to variations of 0.5 [m/s^2], and (ii) smooth lateral maneuvers (e.g., lane changes) by setting $q_{\dot{\theta}}^{(j)} = 0.001$ [rad$^2/s^3$] corresponding to variations of 1.81 [deg/s^2], for both vehicles ($j \in \{1, 2\}$). In the measurement model of the EKF, the precision of the position measurements was set at 0.100 [m] (indicative of DGNSS) and for the inter-vehicle distance measurements at 0.050 [m] (indicative of an automotive-grade LiDAR system). Based on this setup, we have carried out a positioning safety analysis for vehicle 1 by computing the total probability of positioning failure for a worst case-scenario at a single-epoch. To achieve this we have computed first the conditional probabilities of positioning failure under each considered hypothesis where: (i) $\mathcal{H}_0$ is the null hypothesis, (ii) $\mathcal{H}_1$ and $\mathcal{H}_2$ account for 1D unmodelled longitudinal accelerations or decelerations of vehicle 1 and vehicle 2, (iii) $\mathcal{H}_3$ and $\mathcal{H}_4$ account for 2D model misspecifications in the position measurements of vehicles 1 and 2, and (iv) $\mathcal{H}_5$ and $\mathcal{H}_6$ account for 1D model misspecifications in the inter-vehicle distance measurements from both vehicles. The results were shown in Table V, and their verification was presented in Table VI, the relative biases between them being below 3%. Next, assumptions were made on the a-priori probabilities of the hypotheses occurrence $\omega_i = \mathsf{P}(\mathcal{H}_i)$, for $i \in \{0, \ldots, 6\}$, to compute the worst-case total probability of positioning failure

$$\underline{\mathbb{P}}_\mathcal{F}(\mathsf{b}) = 1.4 \cdot 10^{-4} \pm 8.3 \cdot 10^{-7}. \tag{35}$$

This result shows that, in this scenario and the considered models and assumptions, even in a setup of [dm]-level vehicle positioning via a combined EKF and DIA method, the probability is rather large compared to what is considered to be desirable for automotive applications (e.g., [5]).

Secondly, we have considered the case when the dependence between parameter estimation and statistical hypothesis testing is *ignored*. In this situation, the evaluation of (33) is based on the following PDFs

$$f_{\underline{\varepsilon}^o}(\varepsilon|\mathcal{H}_a) = \sum_{a=0}^{n_\mathcal{H}} f_{\underline{\hat{\epsilon}}_i}(\varepsilon|\mathcal{H}_a) \int_{\mathcal{P}_i} f_{\underline{\upsilon}}(\upsilon|\mathcal{H}_a) d\upsilon. \tag{36}$$

where $f_{\underline{\hat{\epsilon}}_i,\underline{\upsilon}}(\epsilon, \upsilon) = f_{\underline{\hat{\epsilon}}_i}(\epsilon) f_{\underline{\upsilon}}(\upsilon)$ for $i \in \{0, \ldots, n_\mathcal{H}\}$. The resulting worst-case total probability of positioning failure is

$$\underline{\mathbb{P}}^o_\mathcal{F}(\mathsf{b}) = 1.2 \cdot 10^{-5} \pm 4.5 \cdot 10^{-8}, \tag{37}$$

which is approximately one order of magnitude *lower* than $\underline{\mathbb{P}}_\mathcal{F}(\mathsf{b})$ in (35). Furthermore, we have extended the positioning safety-analyses by considering multiple configurations between the two vehicles. For most of the configurations the worst-case scenario $\underline{\mathbb{P}}^o_\mathcal{F}(\mathsf{b})$ is overly-optimistic. Therefore, ignoring the dependence between parameter estimation and statistical hypothesis testing can result in wrongful positioning safety assessments, such as concluding that safety requirements or guidelines are met when they are not. The conclusion about the consequence of ignoring the aforementioned dependence is consistent with existing research from various other disciplines such as, mathematical statistics, econometrics, and signal processing [17], [18], [19], [20], [21], [22], [23], [24]. We also note that addressing more complex vehicle scenarios—planned as future work—will increase the dimensionality of vector spaces (e.g., the predicted residual space $\mathbb{R}^m$ if additional sensors are used in the vehicle's positioning system), and therefore an increase in the computation times to determine the probability of positioning failure. While these computations are expected to remain feasible offline within a scenario-based safety framework, future work includes also studying computation times for more complex scenarios.

Below we provide several remarks and recommendations regarding positioning safety analyses:

- Any procedure which uses parameter or state estimation and statistical hypothesis testing should consider the dependence between them either through a rigorous theoretical framework or through conservative assumptions which ensure that the conditional PDFs are overbounded with simpler PDFs (e.g., normal distributions).
- We recommend the *distributional theory for the DIA method*, a theoretical framework that rigorously addresses the aforementioned dependence and which gives access to the PDFs conditioned on the statistical hypothesis testing outcome [14].
- The probability of positioning failure should be formulated based on the conditional PDFs. Doing so, a component-wise positioning safety analysis starting from (15) is made possible.
- If a quantity requires numerical simulation (e.g., via Monte Carlo methods) such as the probabilities of the events in (11)-(13) or the probabilities of positioning failure in (33), the simulation uncertainty (e.g., simulation standard deviation) should be quantified and reported.

APPENDIX
THE EXPRESSIONS OF L_i FOR $i > 0$

For model misspecifications in the motion model

$$L_i = (I_n - P^{-1}A^T Q_{\nu\nu}^{-1}A)\Phi\, C_i \underbrace{(-A\Phi\, C_i)^+}_{(C_i^*)^+},$$

$$\left(C_i^*\right)^+ = \left(\left(C_i^*\right)^T Q_{\nu\nu}^{-1}\left(C_i^*\right)\right)^{-1}\left(C_i^*\right)^T Q_{\nu\nu}^{-1}. \tag{38}$$

Similarly, it follows that for model misspecifications in the measurement model we obtain

$$L_i = P^{-1}A^T Q_{\nu\nu}^{-1} C_i C_i^+,$$
$$C_i^+ = \left(C_i^T Q_{\nu\nu}^{-1} C_i\right)^{-1} C_i^T Q_{\nu\nu}^{-1}\ . \tag{39}$$

where $C_i C_i^+ = \mathbf{Q}_{C_i}$.

ACKNOWLEDGMENT

The authors acknowledge the use of computational resources of the DelftBlue supercomputer, provided by Delft High Performance Computing Centre (https://www.tudelft.nl/dhpc).

REFERENCES

[1] P. J. G. Teunissen and O. Montenbruck, Eds., *Springer Handbook of Global Navigation Satellite Systems*. Cham, Switzerland: Springer, 2017.

[2] Y. T. J. Morton et al., Eds., *Position, Navigation, and Timing Technologies in the 21st Century: Integrated Satellite Navigation, Sensor Systems, and Civil Applications*. Hoboken, NJ, USA: Wiley, 2020.

[3] H. Jing, Y. Gao, S. Shahbeigi, and M. Dianati, "Integrity monitoring of GNSS/INS based positioning systems for autonomous vehicles: State-of-the-art and open challenges," *IEEE Trans. Intell. Transp. Syst.*, vol. 23, no. 9, pp. 14166–14187, Sep. 2022.

[4] *Minimum Operational Performance Standards (MOPS) for Global Positioning System/Satellite-Based Augmentation System Airborne Equipment*, document DO-229F RTCA-Special Committee 159, Radio Technical Commission for Aeronautics, 2020, p. 15.

[5] T. G. R. Reid et al., "Localization requirements for autonomous vehicles," in *Proc. SAE Int. J CAV*, vol. 2, no. 3, 2019, pp. 173–190.

[6] K. Jin, H. Kim, S. Ryu, S. Kim, and J. Park, "An approach to constructing effective training data for a classification model to evaluate the reliability of a passive safety system," *Rel. Eng. Syst. Saf.*, vol. 222, Jun. 2022, Art. no. 108446.

[7] V. Chabridon, M. Balesdent, J.-M. Bourinet, J. Morio, and N. Gayton, "Evaluation of failure probability under parameter epistemic uncertainty: Application to aerospace system reliability assessment," *Aerosp. Sci. Technol.*, vol. 69, pp. 526–537, Oct. 2017.

[8] M. Shinozuka, "Basic analysis of structural safety," *J. Structural Eng.*, vol. 109, no. 3, pp. 721–740, Mar. 1983.

[9] J. Blanch et al., "Baseline advanced RAIM user algorithm and possible improvements," *IEEE Trans. Aerosp. Electron. Syst.*, vol. 51, no. 1, pp. 713–732, Jan. 2015.

[10] *Advanced RAIM Technical Subgroup Reference Airborne Algorithm Description Document*, document Version 3.1, Working Group C, 2019.

[11] P. Zhao, M. Joerger, X. Liang, B. Pervan, and Y. Liu, "A new method to bound the integrity risk for residual-based ARAIM," *IEEE Trans. Aerosp. Electron. Syst.*, vol. 57, no. 2, pp. 1378–1385, Apr. 2021.

[12] N. Zhu, J. Marais, D. Bétaille, and M. Berbineau, "GNSS position integrity in urban environments: A review of literature," *IEEE Trans. Intell. Transp. Syst.*, vol. 19, no. 9, pp. 2762–2778, Sep. 2018.

[13] G. Gottschalg, M. Becker, and S. Leinen, "Integrity concept for sensor fusion algorithms used in a prototype vehicle for automated driving," in *Proc. Eur. Navigat. Conf. (ENC)*, Nov. 2020, pp. 1–10.

[14] P. J. G. Teunissen, "Distributional theory for the DIA method," *J. Geodesy*, vol. 92, no. 1, pp. 59–80, Jan. 2018.

[15] S. Zaminpardaz, P. J. G. Teunissen, and C. C. J. M. Tiberius, "Risking to underestimate the integrity risk," *GPS Solutions*, vol. 23, no. 2, pp. 1–16, Apr. 2019.

[16] S. Zaminpardaz and P. J. G. Teunissen, "On the computation of confidence regions and error ellipses: A critical appraisal," *J. Geodesy*, vol. 96, no. 2, pp. 1–18, Feb. 2022.

[17] T. A. Bancroft, "On biases in estimation due to the use of preliminary tests of significance," *Ann. Math. Statist.*, vol. 15, no. 2, pp. 190–204, Jun. 1944.

[18] S. Sarkadi, "Estimation after selection," in *Studia Scientarium Mathematicarum Hungarica*. Budapest, Hungary: Akademiai Kiado the Publishing House of the Hungarian Academy of Sciences, 1967, pp. 341–350.

[19] N. L. Hjort and G. Claeskens, "Frequentist model average estimators," *J. Amer. Stat. Assoc.*, vol. 98, no. 464, pp. 879–899, Dec. 2003.

[20] S. T. Buckland, K. P. Burnham, and N. H. Augustin, "Model selection: An integral part of inference," *Biometrics*, vol. 53, no. 2, p. 603, Jun. 1997.

[21] H. Leeb and B. M. Pötscher, "The finite-sample distribution of post-model-selection estimators and uniform versus nonuniform approximations," *Econ. Theory*, vol. 19, no. 1, pp. 100–142, Feb. 2003.

[22] H. Leeb and B. M. Pötscher, "Model selection and inference: Facts and fiction," *Econ. Theory*, vol. 21, no. 1, pp. 21–59, Feb. 2005.

[23] D. Danilov and J. R. Magnus, "On the harm that ignoring pretesting can cause," *J. Econometrics*, vol. 122, no. 1, pp. 27–46, Sep. 2004.

[24] T. Routtenberg and L. Tong, "Estimation after parameter selection: Performance analysis and estimation methods," *IEEE Trans. Signal Process.*, vol. 64, no. 20, pp. 5268–5281, Oct. 2016.

[25] C. Rose, J. Britt, J. Allen, and D. Bevly, "An integrated vehicle navigation system utilizing lane-detection and lateral position estimation systems in difficult environments for GPS," *IEEE Trans. Intell. Transp. Syst.*, vol. 15, no. 6, pp. 2615–2629, Dec. 2014.

[26] S. Verhagen and P. J. G. Teunissen, "Least-squares estimation and Kalman filtering," in *Springer Handbook of Global Navigation Satellite Systems*, P. J. G. Teunissen and O. Montenbruck, Eds., Cham, Switzerland: Springer, 2017, pp. 639–660.

[27] I. Gillissen and I. A. Elema, "Test results of DIA: A real-time adaptive integrity monitoring procedure, used in an integrated navigation system," *Int. Hydrographic Rev.*, vol. 73, no. 1, pp. 75–103, 1996.

[28] S. Riedmaier, T. Ponn, D. Ludwig, B. Schick, and F. Diermeyer, "Survey on scenario-based safety assessment of automated vehicles," *IEEE Access*, vol. 8, pp. 87456–87477, 2020.

[29] *New Assessment/Test Method for Automated Driving (NATM) Guidelines for Validating Automated Driving Systems (ADS)*, U.N.E.C.E., United Nations Economic Commission for Europe Inland Transport Committee, Geneva, Switzerland, 2023.

[30] E. de Gelder et al., "TNO street wise: Scenario-based safety assessment of automated driving systems," Netherlands Organisation Appl. Sci. Res. (TNO), The Hague, The Netherlands, White Paper TNO 2024 R10983, 2024.

[31] P. J. G. Teunissen, "Batch and recursive model validation," in *Springer Handbook of Global Navigation Satellite Systems*, P. J. G. Teunissen and O. Montenbruck, Eds., Cham, Switzerland: Springer, 2017, ch. 24, pp. 687–720.

[32] W. Baarda, *A Testing Procedure for Use in Geodetic Networks*, vol. 9. Delft, The Netherlands: Netherlands Geodetic Commission, 1968, pp. 1–97.

[33] M. A. Salzmann, *Least Squares Filtering and Testing for Geodetic Navigation Applications*, vol. 37. Delft, The Netherlands: Netherlands Geodetic Commission, 1993, pp. 1–218.

[34] P. J. G. Teunissen and A. Khodabandeh, "BLUE, BLUP and the Kalman filter: Some new results," *J. Geodesy*, vol. 87, no. 5, pp. 461–473, May 2013.

[35] S. Zaminpardaz and P. J. G. Teunissen, "Detection-only versus detection and identification of model misspecifications," *J. Geodesy*, vol. 97, no. 6, pp. 1–19, Jun. 2023.

[36] T. Willke, P. Tientrakool, and N. Maxemchuk, "A survey of inter-vehicle communication protocols and their applications," *IEEE Commun. Surveys Tuts.*, vol. 11, no. 2, pp. 3–20, 2nd Quart., 2009.

[37] M. Boban and P. M. d'Orey, "Exploring the practical limits of cooperative awareness in vehicular communications," *IEEE Trans. Veh. Technol.*, vol. 65, no. 6, pp. 3904–3916, Jun. 2016.

[38] S. Sivaraman and M. M. Trivedi, "Looking at vehicles on the road: A survey of vision-based vehicle detection, tracking, and behavior analysis," *IEEE Trans. Intell. Transp. Syst.*, vol. 14, no. 4, pp. 1773–1795, Dec. 2013.

[39] X. Rong Li and V. P. Jilkov, "Survey of maneuvering targettracking. Part I: Dynamic models," *IEEE Trans. Aerosp. Electron. Syst.*, vol. 39, no. 4, pp. 1333–1364, Oct. 2003, doi: 10.1109/taes.2003.1261132.

[40] M. Tsogas, A. Polychronopoulos, and A. Amditis, "Unscented Kalman filter design for curvilinear motion models suitable for automotive safety applications," in *Proc. 7th Int. Conf. Inf. Fusion*, Jul. 2005, p. 8.
[41] R. Schubert, E. Richter, and G. Wanielik, "Comparison and evaluation of advanced motion models for vehicle tracking," in *Proc. 11th IEEE Int. Conf. Inf. Fusion*, Jun. 2008, pp. 1–6.
[42] P. J. G. Teunissen, *Dynamic Data Processing: Recursive Least-Squares* (Series on Mathematical Geodesy and Positioning). Delft, The Netherlands: Delft Univ. Press, 2001.
[43] European Commission. (2018). *European Road Safety Report: Motorways*. [Online]. Available: https://road-safety.transport.ec.europa.eu/system/files/2021-07/ersosynthesis2018-motorways.pdf
[44] *European Vehicle Market Statistics: Pocketbook 2022–23*, The International Council on Clean Transportation, Washington, DC, USA, 2023.
[45] Wikimedia Commons. *Citroen C3, Top*. Accessed: Apr. 15, 2024. [Online]. Available: https://commons.wikimedia.org/wiki/File:C3top.png#file
[46] G. Genta, "Motor vehicle dynamics: Modelling and simulation," in *Series of Advances in Mathematics for Applied Sciences*, vol. 43. Singapore: World Scientific, 1997, ch. 4, pp. 171–178, doi: 10.1142/3329.
[47] A. Kealy and T. Moore, "Land-based applications of GNSS," in *Springer Handbook of Global Navigation Satellite Systems*, P. J. G. Teunissen and O. Montenbruck, Eds., Cham, Switzerland: Springer, 2017, ch. 2, pp. 841–856.
[48] Y. Feng, C. Wang, and C. Karl, "Determination of required positioning integrity parameters for design of vehicle safety applications," in *Proc. Int. Tech. Meeting Inst. Navigat.*, Feb. 2018, pp. 129–141.
[49] O. N. Kigotho and J. H. Rife, "Comparison of rectangular and elliptical alert limits for lane-keeping applications," in *Proc. ION GNSS+, Int. Tech. Meeting Satell. Division Inst. Navigat.*, Oct. 2021, pp. 93–104.
[50] S. N. Afriat, "Orthogonal and oblique projectors and the characteristics of pairs of vector spaces," *Math. Proc. Cambridge Phil. Soc.*, vol. 53, no. 4, pp. 800–816, Oct. 1957.
[51] A. Bjorck and G. H. Golub, "Numerical methods for computing angles between linear subspaces," *Math. Comput.*, vol. 27, no. 123, p. 579, Jul. 1973.
[52] A. V. Knyazev and M. E. Argentati, "Principal angles between subspaces in an A-based scalar product: Algorithms and perturbation estimates," *SIAM J. Sci. Comput.*, vol. 23, no. 6, pp. 2008–2040, Jan. 2002.
[53] J. Martins et al., "Defining a braking probability to estimate extreme braking forces on road bridges," in *Proc. 12th Int. Conf. Appl. Statist. Probab. Civil Eng. (ICASP)*, 2015.
[54] *GPS Standard Positioning Service Performance Standard*, 5th ed., U.S. Department of Defense, Arlington County, VA, USA, 2020, pp. 1–196.
[55] A. Richter et al., "Components and their failure rates in autonomous driving," in *Proc. 33rd Eur. Saf. Rel. Conf.*, 2023, pp. 233–240.
[56] *Delft High Performance Computing Centre*, Delft Supercomputer (Phase 1), Delft, The Netherlands, 2022.

Sebastian Ciuban received the M.Sc. degree in aerospace systems: navigation and telecommunications from the École Nationale de l'Aviation Civile (ENAC), Toulouse, France, in 2017. He is currently pursuing the Ph.D. degree in GNSS safe-positioning for automated and autonomous vehicles with Delft University of Technology, Delft, The Netherlands. After his M.Sc. degree, he joined European Space Research and Technology Centre (ESTEC), as a Young Graduate Trainee (YGT) with the Directorate of Navigation. From 2019 to 2021, he was a GNSS Engineer with CGI Nederland B.V. His research interests include the interplay between parameter estimation and statistical hypothesis testing, numerical integration methods, and safety-analyses of positioning systems.

Peter J. G. Teunissen (Senior Member, IEEE) is currently a Professor of geodesy and satellite navigation with Delft University of Technology, The Netherlands, and a member with the Royal Netherlands Academy of Arts and Sciences. His past academic positions include the Head of Delft Earth Observation Institute, the Science Director of Australian Centre for Spatial Information, and a Federation Fellow of Australian Research Council. He has been research-active in various fields of Earth observation, with current research focused on the development of theory, models, and algorithms for high-accuracy applications of satellite navigation and remote sensing systems.

Christian C. J. M. Tiberius received the Ph.D. degree in recursive data processing for kinematic GPS surveying from Delft University of Technology, Delft, The Netherlands, in 1998. He is currently an Associate Professor with the Geoscience and Remote Sensing (GRS) Department, Delft University of Technology. His research interests include navigation, with GNSS and terrestrial radio positioning, primarily for automotive applications.